








A Newly Synthesized β -amino- α , β -unsaturated Ketone Derivative of β -himachalene: Structural, NBO, NLO, and Molecular Docking Studies

Mustapha Ait El Had ^{1,2,3*} , Mouhi Eddine Hachim ⁴ , Said Byadi ⁵ , Lahoucine Bahsis ^{4,6*} , Abdelouahd Oukhrib ¹, Hafid Anane ⁴ , Lahcen El Ammari ⁷ , Mohamed Saadi ⁷ , Moha Berraho ¹, Ahmed Benharref ¹, Moha Taourirte ²

¹ Laboratory of Chemistry of Natural Substances, Faculty of Sciences Semlalia, Cadi Ayyad University, B.P. 2390, Marrakech, Morocco, mustapha.aitelhad20@gmail.com (M.A.), oukhrib@gmail.com (A.O.), berrahomoha7@gmail.com (M.B.), a.benharref@gmail.com (A.B.);

² Laboratory of Sustainable Development and Health Research, Faculty of Science and Technology of Marrakech (FSTGM), Cadi Ayyad University Marrakech, 40000 Marrakech, Morocco, mustapha.aitelhad20@gmail.com (M.A.), taourirte@gmail.com (M.T.);

³ Laboratory of Natural Products and Applied Organic Synthesis, Department of Organic Chemistry, Faculty of Sciences, University of Granada, 18071 Granada, Spain, mustapha.aitelhad20@gmail.com (M.A.);

⁴ Laboratory of Analytical and Molecular Chemistry, Polydisciplinary Faculty, Cadi Ayyad University, BP 4162, 46000 Safi, Morocco, mouhieddinehachim@gmail.com (M.E.H.), bahsis.lahoucine@gmail.com (L.B.), ananehafid@gmail.com (A.H.);

⁵ Extraction and Valorization Spectroscopy Team, Organic Synthesis, Extraction and Valorization Laboratory, Faculty of Sciences of Ain Chock, Hassan II University, Casablanca, Morocco, saidbyadii@gmail.com (S.B.);

⁶ Laboratory of Coordination and Analytical Chemistry, Department of Chemistry, Faculty of Sciences of El Jadida, Université Chouaïb Doukkali, B.P.: 20, El Jadida 24000, Morocco, bahsis.lahoucine@gmail.com (L.B.);

⁷ Laboratoire de Chimie Appliquée des Matériaux, Centre des Sciences des Matériaux, Faculty of Science, Mohammed V University in Rabat, Avenue Ibn Battouta, BP 1014 Rabat, Morocco; l_ellammari@yahoo.fr (L.A.), m.saadi6@yahoo.fr (M.S.);

* Correspondence: mustapha.aitelhad20@gmail.com (M.A.); bahsis.lahoucine@gmail.com (L.B.).

Scopus Author ID 57200694391 (L.B.)

Received: 27.11.2021; Accepted: 6.01.2022; Published: 12.02.2022

Abstract : In the current study, a new β -amino- α , β -unsaturated ketone-based himachalene ((1S,3R,8R)-9-amino-2,2-dichloro-3,7,7,10-tetramethyltricyclo[6.4.0.01,3]dodec-9-en-11-one) (4) was synthesized from β -himachalene (1) extracted from essential oil of Atlas Cedar. The β -amino- α , β -unsaturated ketone product (4) was characterized by 1D NMR (¹H, ¹³C) and 2D NMR (HSQC, COSY, NOESY), FTIR analysis, and single-crystal X-ray diffraction. The title compound, C₁₆H₂₃Cl₂NO, crystallizes with two molecules in the asymmetric unit with similar conformations. One of the two molecules is characterized by chlorine and one-methyl position disorder. In the crystal, intermolecular N—H...O hydrogen bonds lead to forming a three-dimensional framework. In addition, the molecular structure of the title compound was examined by Hirshfeld topology analysis and Density Functional Theory (DFT) using B3LYP calculations at 6-311+G(d,p) level. The optimized structure parameters were compared with the experimental result, an excellent correlation between theoretical structures parameters and experimental values was found. The natural bond orbitals (NBO) analysis and the first-order hyperpolarizability were also performed. Moreover, two biological activities were examined for product 4 against Acetylcholinesterase and Cytochrome P450 3A4, which bind to similar fragments with molecular docking. We find good scores and binding affinity of our molecule to link to these two proteins.

Keywords: β -himachalene; β - amino ketone; NLO; DFT calculation; X-ray diffraction; molecular docking.

© 2022 by the authors. This article is an open-access article distributed under the terms and conditions of the Creative Commons Attribution (CC BY) license (<https://creativecommons.org/licenses/by/4.0/>).

1. Introduction

Himachalene compounds represent Atlas cedar's main component of essential oil [1–4]. They are an excellent source of raw material for several industrial processes to synthesize new molecules with a broad spectrum of pharmacological properties [5,6]. Consequently, considerable efforts have been devoted to designing and synthesizing a wide range of himachalene derivatives [6–10]. The researchers have reported diverse pharmaceutical activities for himachalene derivative compounds such as anticancer, antifungal, antitumor, and anti-inflammatory [11–18]. The interest himachalene in biological applications has received significant attention in the last two decades [19–23]. Likewise, chlorinated products were reported in the literature for significant biological multi-activity, such as improving PET radiotracer in imaging P-gp function [24], mitochondrial-specific reporters [25], antiplasmodium agents [26], and drugs for the treatment of COVID-19 patients [27]. Moreover, the molecules based on 8,8-dichlorobicyclo[5.1.0]octane are very important as potential multidrug for resistance reversal agents [28] and inhibition of verapamil binding [29]. Similarly, the dechlorinated α , β -unsaturated ketone, has antimicrobial activity against the bacterium *Staphylococcus aureus* [30,32]. On the other hand, β -amino- α , β -unsaturated ketones analogs displayed potent anticonvulsant, neuronal and antibacterial activities [33,36].

As part of our ongoing interest in himachalene valorization, we have reported the synthesis of new himachalene derivatives [37–41]. Taking into account all the above data, we present herein the synthesis of a new compound-based himachalene, namely (1S,3R,8R)-9-amino-2,2-dichloro-3,7,7,10-tetramethyltricyclo[6.4.0.0^{1,3}]dodec-9-en-11-one (**4**). This compound can be obtained from β -himachalene (**1**) in three steps. Firstly, gem-dihalogenocyclopropanation of β -himachalene, The study of this step theoretically in regioselectivity has been reported in the literature. [42] allylic oxidation gives α , β -unsaturated ketone intermediate (**3**) [43]. The latter was reacted with sodium azide at room temperature in dichloromethane to obtain β -amino- α , β -unsaturated ketone (**4**). The molecular structure was determined by ¹H, ¹³C NMR, FT-IR spectra and was confirmed by X-ray crystallography analysis. NBO and NLO analysis were performed using DFT/B3LYP method at 6-311+G(d,p) level. Moreover, two biological activities were examined for compound 4, against Acetylcholinesterase and Cytochrome P450 3A4, which are known to bind to similar fragments with molecular docking.

2. Materials and Methods

All chemicals and solvents were purchased from Merck. Thin-layer chromatography (TLC) was performed using F254 percolated plates (0.25 mm) and visualized by UV fluorescence quenching and phosphomolybdic acid solution staining. The chromatography separations were carried out on silica gel 60 (230-400 Mesh) using a conventional column, using Hexane-AcOEt. ¹H and ¹³C NMR spectra were recorded at 500 and 126 MHz, respectively, on Bruker (Avance Neo) with the program (TopSpin-4.07). Infrared spectra spectrums (IR) were recorded on an FTIR spectrophotometer (Nicolet spectrometer (Magna

550)) and are reported in the frequency of absorption (cm^{-1}). ($[\alpha]_D$) measurements were carried out in a polarimeter, utilizing a 1 dm length cell and CHCl_3 as a solvent. Concentration is expressed in mg/mL.

The products, dichloro-cyclopropane (**2**) and enondichloro (**3**) were prepared according to the protocol described in the literature [42, 43].

2.1. Procedure for the synthesis of compound 4.

Compound 4 (Scheme 1) was prepared according to our described protocol [44]. The compound ((1S,3R,8R)-2,2-dichloro-3,7,7,10-tetramethyltricyclo[6.4.0.0^{1,3}]dodec-9-en-11-one) (**3**) (280 mg, 0.91 mmol) was dissolved in CH_2Cl_2 (5 mL) and trifluoroacetic acid $\text{CF}_3\text{CO}_2\text{H}$ (4 mL) at 0 ° C. Then, the sodium azide (178 mg, 2.73 mmol) was added to the reaction mixture and stirred at room temperature for 18 hours. After completion, the reaction mixture was neutralized and washed with a saturated solution of Na_2CO_3 (3 x 15 mL) and then extracted with ethyl acetate (3 x 15 mL). The combined organic phases were dried on anhydrous sodium sulfate (Na_2SO_4). After removing the solvent, the product was purified by flash column chromatography on silica gel with eluent EtOAc/hexane (3/7). The product (**4**) was obtained with 58% (87 mg, 287 μmol) yield as white solid.

$[\alpha]_D^{25} = -44.9$ (c 4.8, CHCl_3). ^1H NMR (500 MHz, Chloroform-d, $\delta = \text{ppm}$): 0.87 (s, 3H), 1.17 (s, 3H), 1.18 (s, 3H), 1.35 (ddd, J = 14.1, 4.9, 2.4 Hz, 1H), 1.62 (td, J = 13.7, 12.2, 3.5 Hz, 1H), 1.68 – 1.81 (m, 2H), 1.75 (s, 3H), 1.71 – 1.91 (m, 2H), 2.48 (s, 1H), 2.50 (d, J = 18.6 Hz, 1H), 2.63 (d, J = 18.6 Hz, 1H), 4.79 (br s, 2H). ^{13}C NMR (126 MHz, Chloroform-d, $\delta = \text{ppm}$): 7.79 (CH_3), 15.29 (CH_3), 20.79 (CH_2), 27.68 (CH_3), 28.93 (CH_2), 29.80 (CH_2), 30.76 (CH_3), 32.6 (C), 34.63 (C), 35.31 (CH_2), 38.02 (C), 49.44 (CH), 76.79 (C), 106.84 (C), 160.71 (C-NH₂), 192.75 (C=O). FT-IR (film, cm^{-1}): 3336, 3209, 2930, 1648, 1542, 1455, 1408, 1390, 1366, 1272, 1080, 755.

2.2. X-ray structure determination for compound 4.

The compound (**4**) was dissolved in a diethyl ether and hexane mixture. The resulting solution is maintained at room temperature; slow evaporation of the solvent affords colorless crystal. A suitable single crystal was selected under a microscope, and X-ray diffraction data were collected on a Bruker D8 VENTURE Super DUO diffractometer using copper radiation. SAINT+ 6.02 program was used for the extraction and integration of diffraction intensities [45], and the SADABS program was carried out to correct the absorption effect [46]. The structure was solved by direct methods, using the (SHELXT) program [47] included in the WINGX package [48], and refined by least-squares against F² (SHELXL-2015) [49]. All non-hydrogen atoms were anisotropically refined, whereas the hydrogen atoms were positioned geometrically and refined using a riding model. Crystal data, data collection, and structure refinement details are summarized in Table 1. The anisotropic displacement parameters and the observed and calculated structure factors (Supplementary materials) are deposited in CCDC 1995106 Data Centre. These data can be obtained free of charge via the Cambridge Crystallographic Data Centre, <https://www.ccdc.cam.ac.uk>.

Table 1. Crystal data, data collection, and structure refinement details for the title compound.

Crystal data	
Chemical formula	C ₁₆ H ₂₃ Cl ₂ NO
Mr	316.25

Crystal data	
Crystal system, space group	Monoclinic, P21
Temperature (K)	296
a, b, c (Å)	7.120 (3), 15.094 (5), 15.407 (5)
β (°)	94.07 (3)
V (Å ³)	1651.6 (10)
Z	4
Radiation type	Cu K α
μ (mm ⁻¹)	3.49
Crystal size (mm)	0.26 × 0.19 × 0.16
Data collection	
Diffractometer	Bruker D8 VENTURE Super DUO
Absorption correction	Multi-scan (SADABS; Krause <i>et al.</i> , 2015)
Tmin, Tmax	0.571, 0.753
No. of measured, independent and observed [I > 2 σ (I)] reflections	23354, 6026, 5610
Rint	0.034
(sin θ / λ)max (Å ⁻¹)	0.608
Refinement	
R[F ² > 2 σ (F ²)], wR(F ²), S	0.040, 0.112, 1.03
No. of reflections	6026
No. of parameters	399
No. of restraints	1
H-atom treatment	H-atom parameters constrained
Δ >max, Δ >min (e Å ⁻³)	0.54, -0.25
Absolute structure	Flack x determined using 2388 quotients [(I+)-(I-)]/[(I+)+(I-)] (Parsons, Flack and Wagner, Acta Cryst. B69 (2013) 249-259).
Absolute structure parameter	0.050 (5)

2.3. Hirshfeld surface analysis.

The visualization of intermolecular interactions in compound (**4**) was carried out by Hirshfeld surface analysis. The Hirshfeld surface [50] and 2D fingerprint [51] plots were explored using the CrystalExplorer17.5 program [52], and the CIF files were used as the input file. Hirshfeld surface was represented by d_e and d_i , which denote the distance from the nearest atom outside and inside of the surface. Both are used to define the normalized contact distance (d_{norm}). For the visualization of d_{norm} , a red-blue-white (RBW) color scale was selected.

2.4. Computational methods.

The entire quantum chemical calculations were performed using the DFT/B3LYP method in coordination with 6-311G+(d, p) basis sets used GAUSSIAN 09 [53]. The optimization of geometries has been performed at the B3LYP/6-311G+(d,p) level of theory. All obtained frequencies are positive, proving that the structure corresponds to minimum energy. The non-linear optical (NLO) was investigated using the calculations of polarizability α and first-order hyperpolarizability β [54–58] on the optimized geometry of 4 compounds within DFT at the DFT B3LYP/6-311+G(d,p) level (see Electronic supplementary material for more details) [59, 60]. In addition, the polar properties of compound **4** and urea were computed. Urea is the prototypical molecule utilized in investigating the NLO properties of the compound. For this reason, urea was often used as a threshold value for comparative purposes.

2.5. Molecular docking.

Molecular docking study is a beneficial cheminformatics tool that gives us information about our compound's possible interactions with proteins related to specific biological activity.

It provides how our molecule interacts with such protein and how a ligand and protein binding interactions with each other, representing a novel approach of drug conception [61, 62].

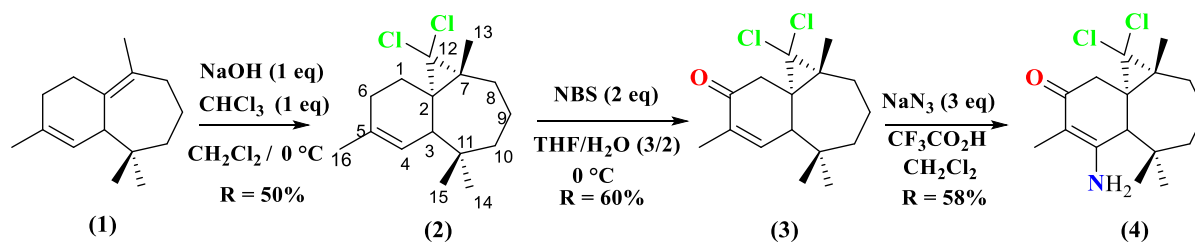
Biological activity of 4 has been evaluated using Maestro software (Schrödinger, LLC, New York, NY, 2018) [63]. In the first place, we used the PASSonline server to predict the biological activity of molecule 4 [64]. We found that the title molecule inhibits the CYP2J2 substrate, predominantly expressed in extrahepatic tissues, especially in the heart, skeletal muscle, kidney, lung, pancreas, bladder, and brain [65–67]. While a crystal structure has yet to be elucidated, molecular modeling recommends structural similarity between CYP2J2 and CYP3A4, explaining why the two enzymes share several substrates of various therapeutic areas, such as the antihistamine drugs terfenadine, astemizole, and ebastine [68–73] anticancer drug tamoxifen, and drugs such as thioridazine or cyclosporine [74–76]. That is why we choose the Crystal structure of human cytochrome P4503A4 bound to inhibitor ritonavir (PDB id 3NXU) characterized by X-ray diffraction with a 2Å of resolution from protein data Bank in Europe (PDBe). We also evaluate the protein's biological activity called Acetylcholinesterase (AChE) as Arulraj Ramalingam *et al.* reported that this protein has been inhibited by compounds similar to our molecule AChE is a crucial enzyme enhancing the cognitive disorder, leading to Alzheimer's disease. Ache inhibition is an important therapeutic mechanism against it. Crystal structure of Recombinant Human Acetylcholinesterase in Complex with Donepezil (PDB id 4EY7) was characterized by X-ray diffraction with a 2.35 Å of resolution from protein data Bank (RCSB PDB).

The compound was initially docked to the binding site CYP3A4 and AChE receptor using Glide XP (Schrödinger Suite 2018) with standard settings. The procedure was composed of preparing the ligand and receptor, grid generation, and docking. Besides, the MM-GBSA method was used to estimate ligand-binding affinities [77–78]. Both catalytic sites of two proteins are predicted to be the nearest space with a distance less than 3 from the ligand crystallized with the protein.

3. Results and Discussion

The β-himachalene (1) is a major constituent of the Atlas cedar's essential oil, representing 50% of the total composition [79–81], which was obtained from the hydrocarbon part after chromatography on silica gel column impregnated with silver nitrate (10%) with hexane as eluent. Their chemical structure is a bicyclic compound with two unsaturated endocyclic bonds. The action of a stoichiometric amount of dichlorocarbene, generated in situ from chloroform using NaOH and chloroform in the presence of tertiary butylammonium (TEBA-Cl) as a phase transfer catalyst in CH₂Cl₂, on himachalene (1), at 0°C to room temperature, leads regio- and stereospecifically, to a (1S,3R,8R)-2,2-Dichloro-3,7,7,10-tetramethyltricyclo[6,4,0,01,3]dodec-9-ene(2) (Scheme 1) [82]. Allylic oxidation of latter (2) by N-Bromosuccinimide (NBS) (2 equivalents), in a mixture of THF/H₂O (60/40) at 0°C leads to the formation of compound (3), (1S,3R,8R)-2,2-Dichloro-3,7,7,10-tetramethyltricyclo[6.4.0.01,3]dodec-9-en-11-one, (60%) yield [83].

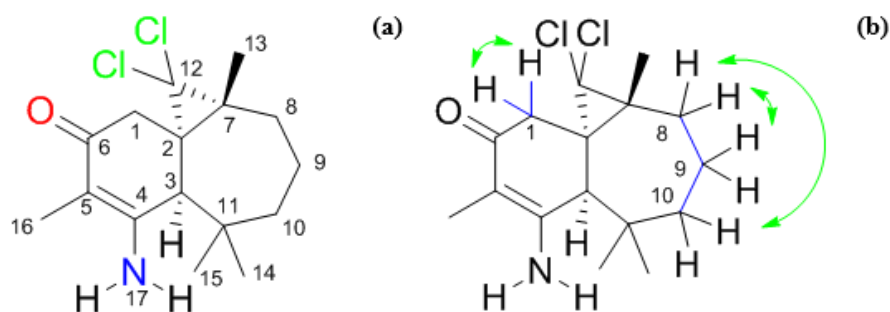
The reaction between compound (3) and an excess of sodium azide with the presence of CF₃CO₂H in dichloromethane at 0°C give β-amino-α,β-unsaturated ketone (1S,3R,8R)-9-amino-2,2-dichloro-3,7,7,10-tetramethyltricyclo[6.4.0.01,3]dodec-9-en-11-one (4) as a new himachalene derivative (Scheme 1).



Scheme 1. Synthesis of compound (4) from β -himachalene (1).

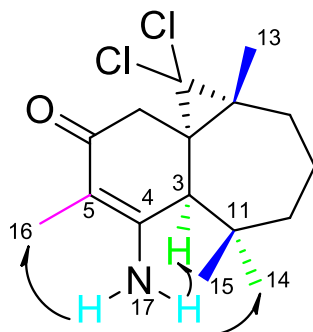
3.1. ^1H , ^{13}C NMR, HSQC, NOESY spectra, and FT-IR analysis of compound (4).

The target product was firstly analyzed by different spectroscopies techniques such as 1D NMR (^1H and ^{13}C NMR), 2D NMR (HSQC, COSY, HMBC (See Figures S2 and S3 in Electronic supplementary material), and NOESY), and IR-FTIR. The analysis ^1H , ^{13}C NMR and HSQC spectra (Figure 1 and 2) of the product (4) showed the presence of 16 carbon signals (Scheme 2a), and the presence of four methyl groups represented by singlets (δH 0.87, δC 27.68, C13; δH 1.16, (15.29 and 30.76), (C14 and C15) and δH 1.75, δC 7.79, C16), also four methylene (δH 1.72, δC 28.93, C-8; δH 1.84, δC 32.60, C9; δH 1.25, δC 29.80, C10), including methylene in α of the ketone (δH (2.50, d, $J = 18.6$ Hz) and (2.63, d, $J = 18.6$ Hz), δC 35.31, C1). One methine singlet (δH 2.48, δC 49.44, C3), and seven quaternary carbons (δC 32.60, C7; δC 38.02, C11; δC 76.79, C12), including two alkenes carbons (δC 160.71, C4; δC 106.84, C5) and one carbonyl carbon (δC 192.75, O=C6).



Scheme 2. Assignment molecule of the product (4).

The spectrum of homonuclear correlation spectroscopy COSY ($1\text{H}-1\text{H}$) showed two structural fragments: $\text{H1}-\text{C}(1)-\text{H1}'$ (δH 2.50, d, $J = 18.6$ Hz and δH 2.63, d, $J = 18.6$ Hz), and $-\text{CH}_2-\text{CH}_2-\text{CH}_2-$ (C8, C9, and C10) as it appears in Scheme 2b.



Scheme 3. Amin group Correlation (NOESY) with Methyl groups Me-14, Me-16, and Methine H-3.

The NMR data information of Heteronuclear Single Quantum Correlation (2D-HSQC) indicates the appearance of a singular peak at δH 2.48 ppm (H3) corresponds to the carbon of δC 49.44 ppm (C3) (Figure 2). With the disappearance of signal the starting product (3), the

doublet quadruplet (dq), which appeared in 6.73 ppm corresponds to the proton of position 4 (Scheme 1), and the transformation of a doublet into a singular ($\delta H=2.75$ ppm), corresponds to the proton of position 3 (H3) (Figure 2). The ^{13}C -NMR analysis shows one carbon with halogen (C-Cl) at ($\delta C=76.79$ ppm).

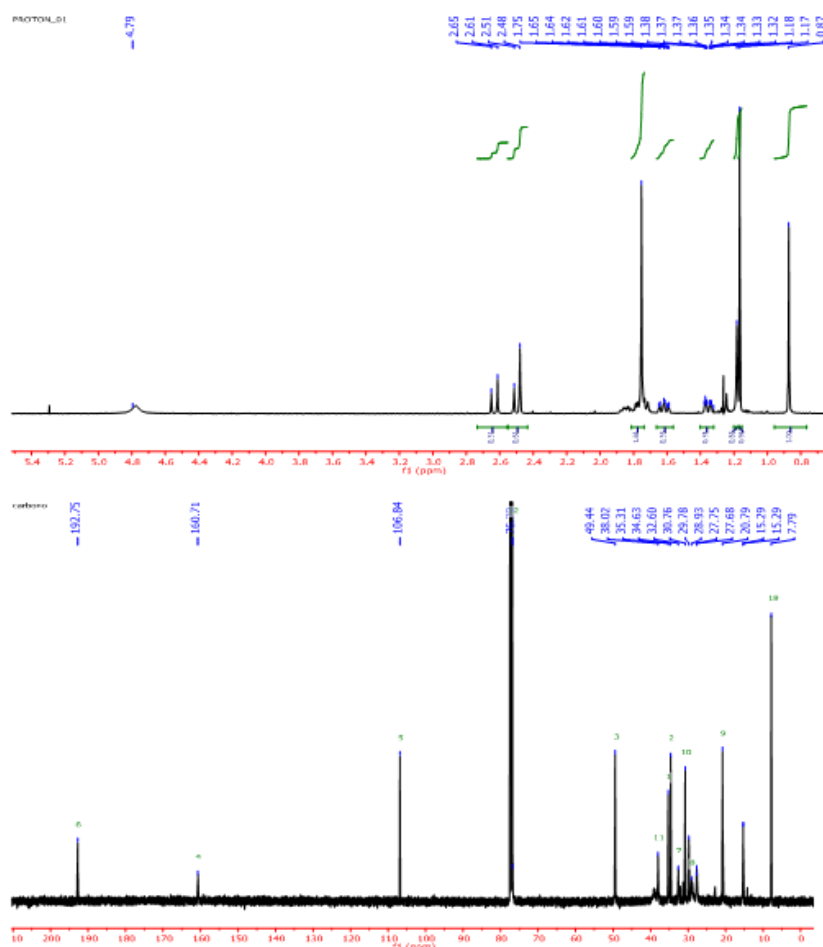


Figure 1. 1H and ^{13}C NMR spectra of the product (4).

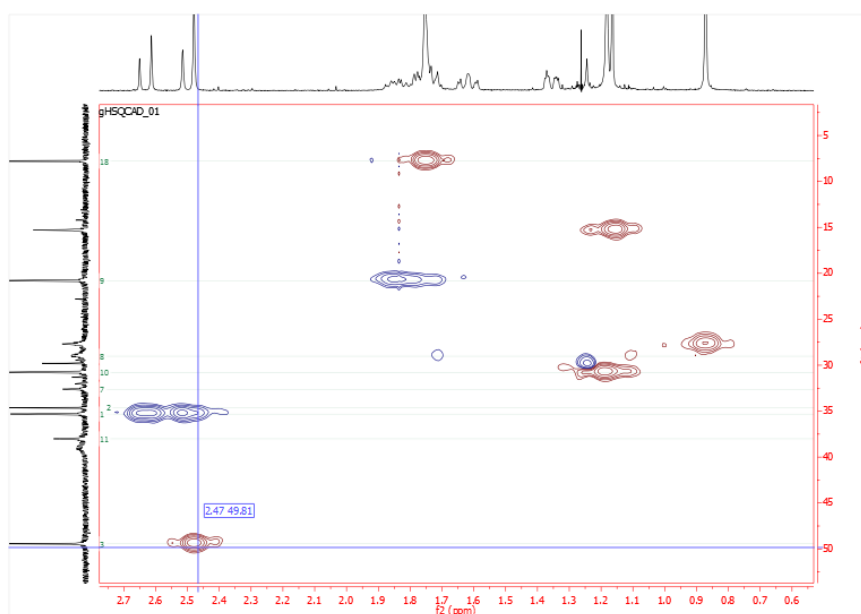


Figure 2. HSQC analysis of compound (4) (correlation of proton the 2.48 ppm with carbon 49.44ppm).

In the 2D-NOESY experiment of compound (4) (Figure 3), H-(N17) ($\delta\text{H}= 4.49$ ppm) correlated with Me-14 ($\delta\text{H}= 1.16$, $\delta\text{C}= 15.29$ ppm), Me-16 ($\delta\text{H}=1.75$, $\delta\text{C}=7.79$ ppm) and Methine H-3 ($\delta\text{H}=2.48$, $\delta\text{C}=49.44$ ppm) but not with Me-13 ($\delta\text{H}=0.87$, $\delta\text{C}=27.68$ ppm) and Me-15, ($\delta\text{H}=1.16$, $\delta\text{C}=30.76$ ppm). These results indicate that amino group (NH_2) is bound to quaternary carbon C4 ($\delta\text{C}=160.71$ ppm), and methyl group Me-14 with H-3 were on the same face of the cycloheptane ring (Scheme 3).

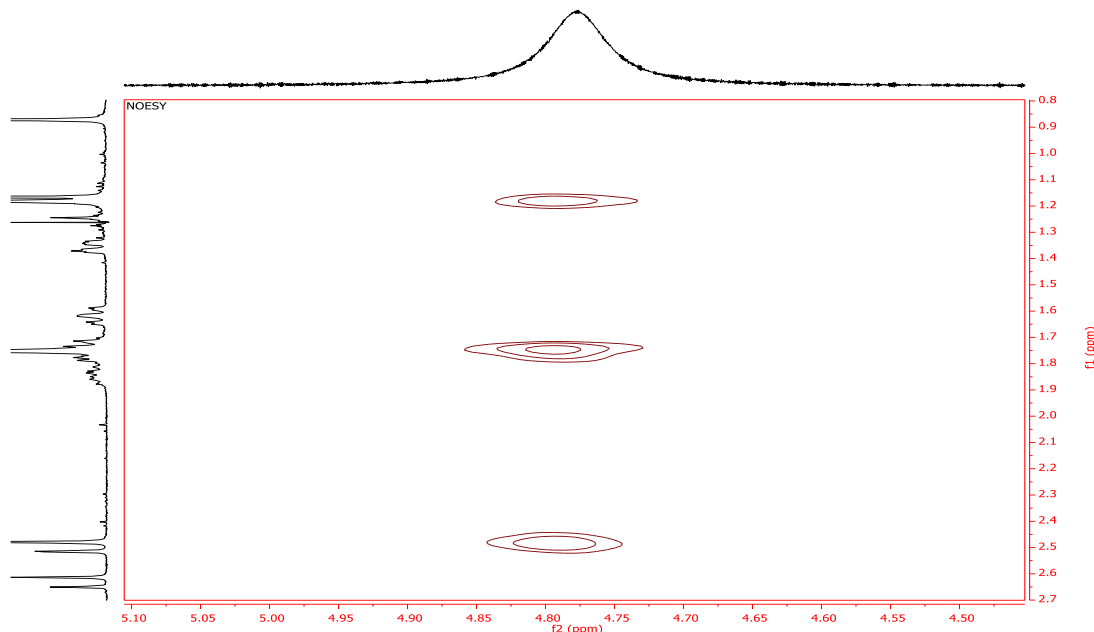


Figure 3. NOESY (Nuclear Overhauser Effect Spectroscopy) analysis of compound (4).

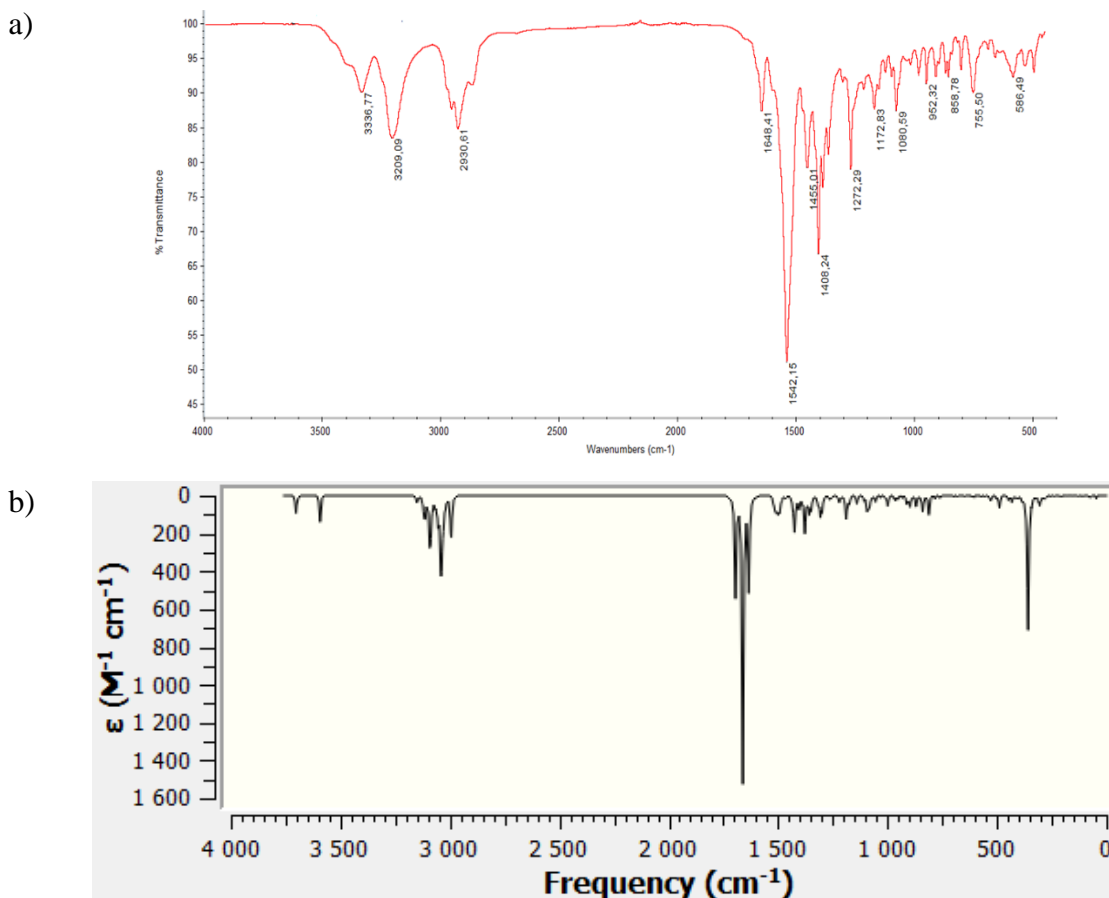


Figure 4. (a) Experimental and (b) theoretical FTIR spectrum of compound (4).

The FT-IR spectrum of compound (4) showed the appearance of the characteristic bands designating the presence of the specific bands of this molecule: The N-H stretching vibrations of sp^3 type were observed at 3336 cm^{-1} (Figure 4), and also the appearance of a band at 1272 cm^{-1} corresponding to the C-N band of a primary amine, which indicates the presence of the amine group NH_2 . The appearance of a strongly intense and fine band around 1542 cm^{-1} due to the stretching vibrations of the non-aromatic C=C band, also the stretching vibrations of the double band C=O, α , β unsaturated has observed at 1648 cm^{-1} . Then, two bands are located at (1366 and 1390 cm^{-1}) and 755 cm^{-1} , which are attributed to the C-C and C-H (methylene $-(\text{CH}_2)_n-$) bands, respectively. The stretching vibrations C-H (alkane) and C-H (methyl group) were observed at 2930 and 1455 cm^{-1} , respectively. Thus, spectrum analysis has shown the stretching vibrations of the C-Cl band at 586.49 cm^{-1} . Subsequently, the scaled harmonic vibrational frequencies of compound 4 were calculated from the optimized structure with DFT/B3LYP using a 6-311G+(d,p) basis. The experimental and theoretical spectrums are shown in Figure 4b. The analysis indicates the band's existence at 3592 cm^{-1} that corresponded to the amine function (NH), the carbonyl group (ketone) band at 1694 cm^{-1} , and the strong band characteristic of the C=C band at 1633 cm^{-1} . In addition, a stretching vibration of the C-Cl band was located at 556 cm^{-1} , indicating a good correlation between computed values and experimental results.

3.2. Single crystal X-ray structural analysis of compound (4).

To confirm the proposed structure by NMR and FTIR analysis, we carried out an X-ray analysis for an appropriate single crystal of the title compound. The plot of the two molecules building the asymmetric unit of this compound is illustrated in Figure 5. The first molecule (O1N1C1C12 C1 to C16) and the second molecule (O2N2C13C14 C17 to C32) showed nearly the same configurations. In fact, the chlorine positions C13 and C14 are divided into C13A, C13B, C14A, C14B and the refinement of the occupancy rates of $\text{C13A} = \text{C14A} / \text{C13B} = \text{C14B}$ leads to (0.631 / 0.369) at the atomic positions. Similarly, the methyl C30 is split into C30A and C30B, and the refinement of the occupancy rates of $\text{C30A} / \text{C30B}$ led to (0.786 / 0.214) at the atomic positions.

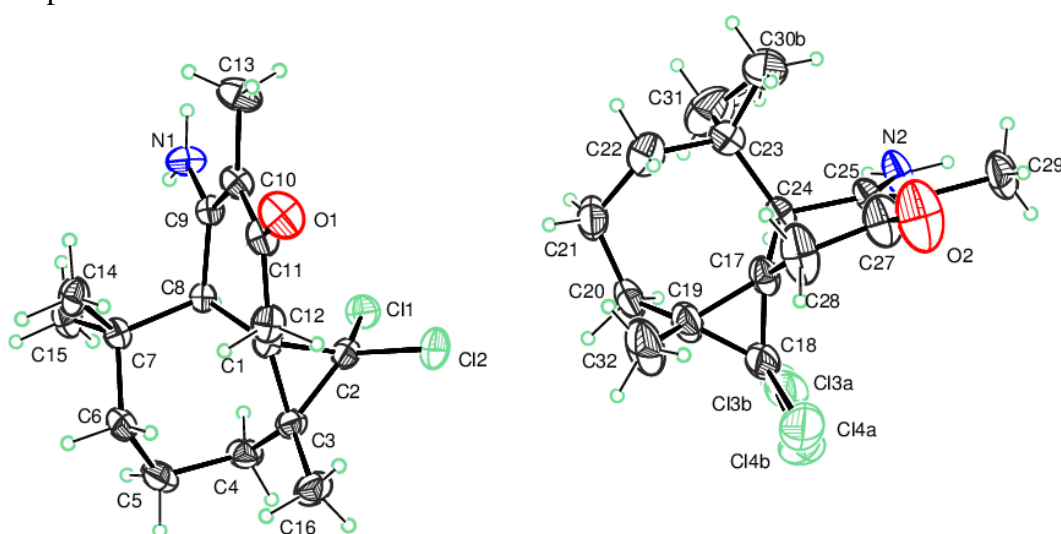


Figure 5. Crystal structure of compound (4), with the atom-labeling scheme. Displacement ellipsoids are drawn at the 30% probability level. H atoms are represented as small circles.

Furthermore, the six-membered rings in the first and second molecules display envelope configurations, with C1 and C17 atoms as a flap, respectively. At the same time, the seven-membered ring adopts a boat configuration in both molecules. Moreover, the dihedral angles between the three-membered cycles and the mean planes through the six-membered rings are $88.1(2)^\circ$ and $86.0(4)^\circ$ in the first and second molecules. In the crystal, molecules are linked together via N-H...O hydrogen bonds to build chains running along the a-axis. Moreover, two intramolecular C-H...Cl hydrogen bonds are also observed in the second molecule. The three-dimensional network of the crystal structure is shown in Figure 6. Owing to the presence of Cl atoms, the absolute configuration of compound 4 (Scheme 1) was found to be C1(S), C3(R), and C8(R) (Figure 5). Indeed, the structure of product (4) was confirmed as (1S,3R,8R)-11-Amino-2,2-Dichloro-3,7,7,10-tetramethyltricyclo [6.4.0.01,3] dodec-10-en-9-one.

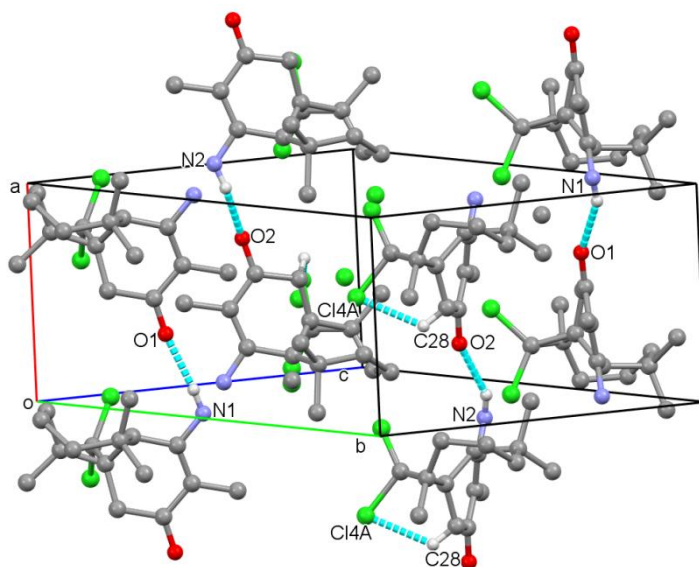


Figure 6. Three-dimensional view of the crystal structure showing the molecules linked through hydrogen bonds as dashed cyan lines.

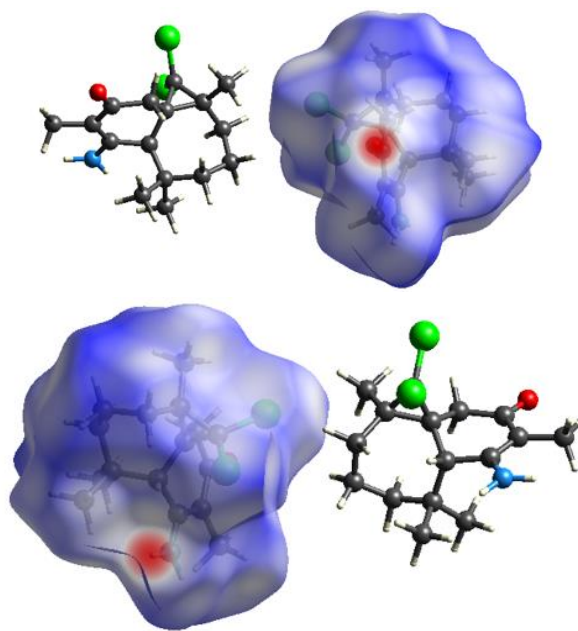


Figure 7. dnorm mapped on the Hirshfeld surfaces for visualizing the intermolecular contacts for the compound 4.

3.3. Hirshfeld surface analysis for compounds 4.

The Hirshfeld surface analysis provides 3D presentations of intermolecular interactions between different units in the crystal packing motifs. The Hirshfeld surface analysis was carried out for the title compound, and the results show the presence of two red regions indicating the interaction that involved hydrogen bonding (Figure 7). The red spot is apparent around the oxygen atom participating in the C-O...H contacts and around the hydrogen atom participating in the N-H...O contacts, with a distance equal 2.03 Å (Table 2). These results are comparable with our finding for the regioselective synthesis of (1S,3R,8R)-11-amino-2,2-dichloro-3,7,7,10-tetramethyltricyclo[6.4.0.01,3]dodec-10-en-9-one in which hydrogen bonding N-H...O is 2.00 Å and D-H...A angle is 159° [83].

Table 2. Hydrogen-bond geometry (Å,°) for compound (4).

D—H...A	D—H	H...A	D...A	D—H...A
C24—H24...Cl3B	0.98	2.48	3.144 (11)	125
C28—H28A...Cl4A	0.97	2.36	2.95 (2)	119
N1—H1B...O1i	0.86	2.03	2.831 (4)	155
N2—H2B...O2i	0.86	2.03	2.808 (5)	151

Further, the 2D-fingerprint plots were investigated to determine the nature and the relative contribution interactions leading to the formation of crystal units (Figure 8). The results show that the significant intermolecular interactions in compound (4) are found for H-H contacts with contributions of 60.3%. The Cl-H/H-Cl contacts are the second-largest contribution to the Hirshfeld surface in both cases with 27.7%, and the O-H/H-O contacts contribute 9.1%. Besides, this analysis shows the presence of intermolecular C-H and N-H interactions, respectively.

3.4. Optimized molecular structure of compound 4.

The optimized geometry of compound 4 (Scheme 1) was performed using DFT at B3LYP/6-311G+(d,p) level, see Figure 9. Selected geometrical parameters were presented in Table 3 and (Table S1 in Electronic supplementary material). The obtained results in XRD and DFT geometry optimization are almost identical, with deviations between the crystalline and X-ray crystallography structures due to differences in the molecular environment [84]. In crystalline structure, the O3-C16, N4-C39, C11-C22, and C12-C22 bond lengths are 1.235, 1.340, 1.762, and 1.762 Å, whereas, in DFT structure, the calculated values are 1.225, 1.375, 1.800, and 1.789 Å, respectively. Similarly, the angle values O3-C16-C17 (122.3/122.84), N4-C39-C17 (121.1/120.99), and C12-C22-C11 (108.02/108.12) computed from the X-ray crystallography/DFT are in close agreement (See Figure S1 in Electronic supplementary material).

3.6. NBO analysis.

Natural bond orbital (NBO) analysis was performed to understand the origin of the intermolecular charge transfer process between electron-donors and electron-acceptors. The hyper conjugative interaction energies were deduced from the second-order perturbation theory analysis of the Fock matrix in the NBO method [85–87].

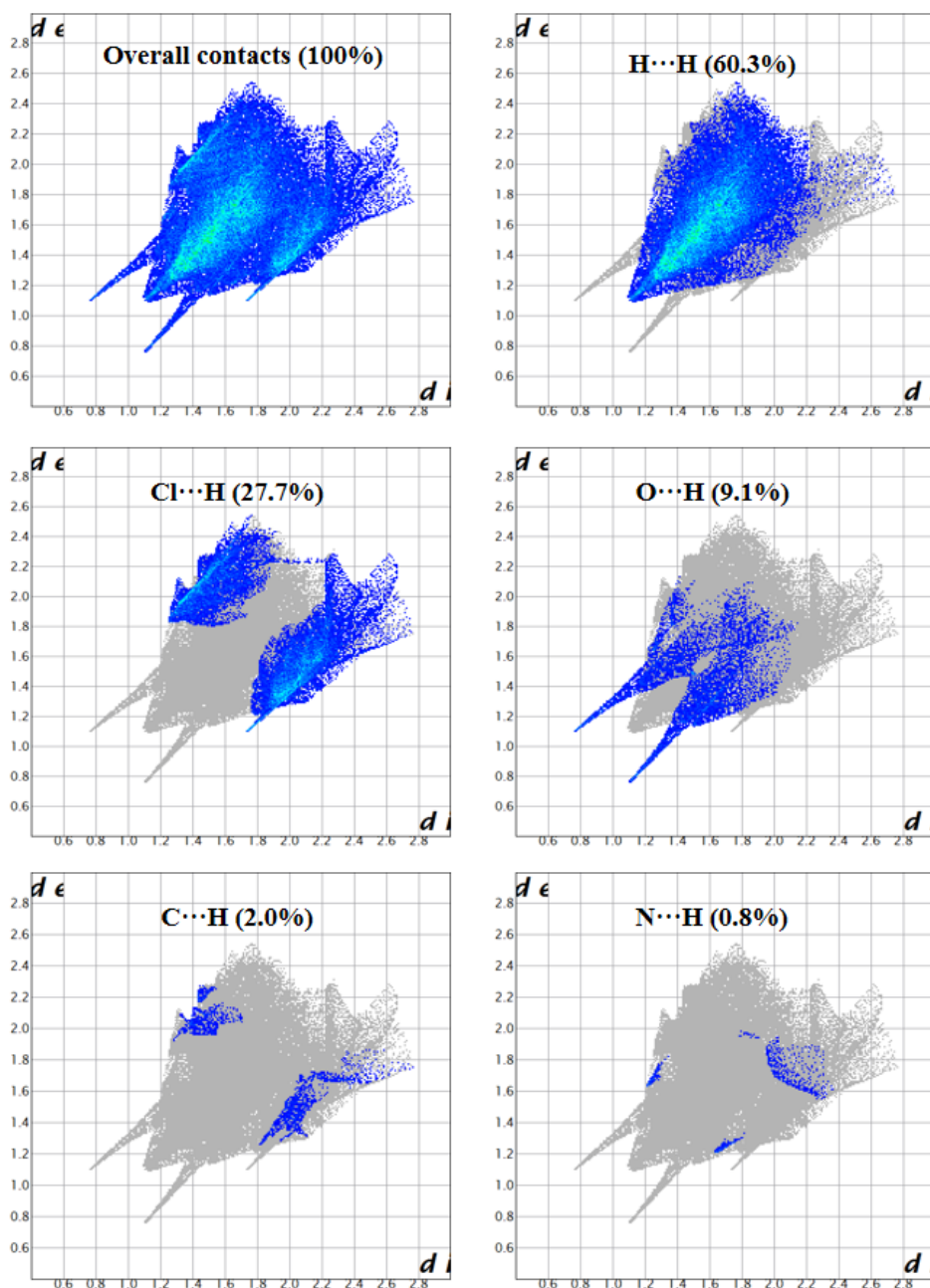


Figure 8. Two-dimensional fingerprint plots for (4).

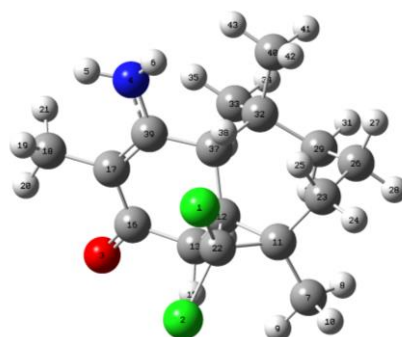


Figure 9. Optimized geometry of product (4) at B3LYP/6-311+G(d,p) level.

For each donor (i) and acceptor (j), the stabilization energy $E^{(2)}$ associated with delocalization i/j is calculated as:

$$E^{(2)} = \Delta E_{ij} = qi \frac{(F_{ij})^2}{(E_j - E_i)}$$

The NBO calculations were performed at the B3LYP/6-311+G(d,p) level, and Table 3 shows the essential donor-acceptor interactions with the highest values of E(2).

Based on the E(2) values reported in Table 3, the electron transfers from one-center lone pair (LP) valance NBO orbitals interactions as LP N4 → σ*(C17-C39), LP O3 → σ*(C13-C16), LP O3 → σ*(C16-C17), LP C12 → σ*(C11-C22) and LP C11 → σ*(C12-C22), with stabilization energies 36.22, 19.83, 17.01, 8.22 and 7.64 kcal/mol, respectively. On the other hand, NBO analysis detected the most probable intermolecular interaction between the binding and anti-adhesion orbitals as π(C17-C39) → π*(O3-C16), σ(C11-C12) → σ*(C11-C22), σ(C12-C22) → σ*(C11-C22), σ(C11-C22) → σ*(C12-C22), σ(C11-C12) → σ*(C12-C22), σ(C13-H14) → π*(O3-C16), σ(C7-H10) → σ*(C11-C12), π(O3-C16) → π*(C17-C39), with stabilization energies 26.29, 9.25, 7.01, 6.75, 6.56, 5.51, 5.29 and 5.21 kcal/mol, respectively. All these findings demonstrate that, NH2 participates an electron-donating group whereas the C=O as an accepting group.

Table 3. Second-order perturbation theory analysis of Fock matrix in NBO basis for compounds (4) and numbering is according to Figure 9.

Donor (i)	Occupancy	Acceptor (j)	Occupancy	E ⁽²⁾ (kcal/mol)	E(j)-E(i) (a.u.)	F(i,j) (a.u.)
π(O3-C16)	1.974	π*(C17-C39)	0.24527	5.21	0.40	0.043
s(N4-H5)	1.986	s*(C37-C39)	0.03025	4.48	1.07	0.062
s(N4-H6)	1.986	s*(C17-C39)	0.02703	3.44	1.30	0.060
s(C7-H8)	1.982	s*(C11-C22)	0.07911	4.77	0.82	0.057
s(C7-H9)	1.988	s*(C11-C23)	0.03007	3.63	0.89	0.051
s(C7-H10)	1.982	s*(C11-C12)	0.05592	5.29	0.82	0.059
s(C11-C12)	1.912	s*(C11-C22)	0.08351	9.25	0.62	0.068
		s*(C12-C22)	0.07058	6.56	0.64	0.058
		s*(C11-C22)	0.07911	3.88	0.85	0.051
		s*(C12-C22)	0.08180	4.16	0.84	0.053
s(C11-C22)	1.951	s*(C11-C12)	0.05592	3.81	0.91	0.053
		s*(C12-C13)	0.03100	4.82	0.99	0.062
		s*(C12-C22)	0.08180	6.75	0.89	0.070
		s*(C12-C37)	0.03426	4.14	0.97	0.057
s(C12-C22)	1.948	s*(C7-C11)	0.02511	4.98	0.97	0.062
		s*(C11-C12)	0.05592	3.94	0.90	0.053
		s*(C11-C22)	0.07911	7.01	0.90	0.071
		s*(C11-C23)	0.03007	3.91	0.97	0.055
s(C13-H14)	1.957	π*(O3-C16)	0.22223	5.51	0.53	0.051
		s*(C12-C22)	0.08180	4.74	0.79	0.055
s(C13-H15)	1.971	s*(C12-C37)	0.03426	4.06	0.88	0.053
s(C16-C17)	1.972	s*(N4-C39)	0.02135	4.93	1.10	0.066
s(C17-C18)	1.977	s*(C37-C39)	0.03025	5.16	1.02	0.065
π(C17-C39)	1.796	π*(O3-C16)	0.22223	26.29	0.30	0.080
s(C18-H20)	1.986	s*(C17-C39)	0.02703	4.74	1.12	0.065
s(C23-H24)	1.975	s*(C11-C12)	0.05592	4.49	0.81	0.054
s(C23-H25)	1.977	s*(C7-C11)	0.02511	3.80	0.88	0.052
s(C26-H28)	1.977	s*(C29-C32)	0.02894	3.92	0.86	0.052
s(C29-H30)	1.976	s*(C32-C40)	0.02117	3.79	0.86	0.051
s(C29-H31)	1.974	s*(C23-C26)	0.01599	3.61	0.86	0.050
		s*(C32-C37)	0.04840	4.45	0.82	0.054
s(C33-H34)	1.986	s*(C32-C37)	0.04840	4.46	0.82	0.055
s(C33-H35)	1.987	s*(C29-C32)	0.02894	3.19	0.86	0.047
s(C33-H36)	1.987	s*(C32-C40)	0.02117	3.43	0.86	0.049
s(C37-H38)	1.965	s*(C12-C13)	0.03100	4.01	0.90	0.054
		s*(C17-C39)	0.02703	3.07	1.14	0.053
s(C37-C39)	1.963	s*(C11-C12)	0.05592	3.05	0.95	0.048
		s*(C17-C18)	0.01799	3.60	1.06	0.055

Donor (i)	Occupancy	Acceptor (j)	Occupancy	E ⁽²⁾ (kcal/mol)	E(j)-E(i) (a.u.)	F(i,j) (a.u.)
		s*(C17-C39)	0.02703	3.31	1.26	0.058
s(C40-H41)	1.986	s*(C32-C37)	0.04840	3.86	0.83	0.051
s(C40-H42)	1.988	s*(C32-C33)	0.01976	3.33	0.88	0.048
s(C40-H43)	1.988	s*(C29-C32)	0.02894	3.33	0.87	0.048
LP C11		s*(C11-C22)	0.07911	3.90	0.64	0.045
		s*(C12-C22)	0.08180	3.66	0.62	0.043
		s*(C12-C22)	0.07058	7.64	0.43	0.051
LP C12		s*(C11-C22)	0.07911	4.14	0.63	0.046
		s*(C12-C22)	0.08180	3.75	0.62	0.043
		s*(C11-C22)	0.08351	8.22	0.41	0.052
LP O3		s*(C13-C16)	0.06125	19.83	0.64	0.102
		s*(C16-C17)	0.06087	17.01	0.75	0.102
LP N4		s*(C17-C39)	0.02703	36.22	0.35	0.100

3.7. Hyperpolarizability calculations.

Synthetic or natural materials' non-linear optical (NLO) proprieties have got great attention due to their rapid response in electro-optic effect and their potentially high nonlinearities. NLO is a crucial function of optical logic, optical modulation, frequency shifting, optical switching, and optical memory for the emerging technologies, and the optical nonlinearity of materials can be amplified either by conjugated bonds or by binding of electron donor and acceptor groups presented in their structures [88–90]. Moreover, the DFT method has been widely used as an efficient method to investigate the NLO materials [60,61]. Hyperpolarizability is very sensitive to the basis sets and level of the theoretical approach employed [91, 92], so the electron correlation can change the value of hyperpolarizability.

The computed hyperpolarizability and dipole moment values obtained from B3LYP/6-311+G(d,p) methods are summarized in Table 4. The first order hyperpolarizability (β total) of 4 with B3LYP/6-311+G(d,p) basis set is 1.906×10^{-30} , three times greater than the value of urea ($\beta_{tot} = 0.620 \times 10^{-30}$ esu).

Table 4. The values of calculated dipole moment $\mu(D)$, polarizability (α_0), first-order hyperpolarizability (β_{tot}) components of 4 and urea.

Parameters	Compound 4	Urea	Parameters	Compound 4	Urea
μ_x	0.188	-0.0004	β_{xxx}	49.978	0.002
μ_y	2.380	-1.529	β_{xxy}	0.824	39.991
μ_z	0.985	-0.002	β_{xyy}	34.540	-0.008
μ	6.564	3.885	β_{yyy}	103.716	-79.123
α_{xx}	194.611	37.201	β_{zxx}	26.922	-0.014
α_{xy}	5.280	0.001	β_{xyz}	53.665	1.427
α_{yy}	203.170	39.680	β_{zyy}	40.998	-0.008
α_{xz}	-2.678	0.281	β_{xzz}	128.987	-0.003
α_{yz}	14.517	0.0002	β_{yzz}	-52.943	-32.687
α_{zz}	185.741	24.527	β_{zzz}	-88.983	-0.016
$\alpha_0(e,s,u)10^{-23}$	0.277	0.209	$\beta_{tot}(e,s,u) 10^{-30}$	1.906	0.620
$\alpha(e,s,u)10^{-23}$	2.883	0.501			

The results indicate the high values of the hyperpolarizabilities of the title molecule are probably attributed to the charge transfer existing amide the benzene rings within the molecular skeleton (Figure 9). This is evidence of the non-linear optical (NLO) property of the molecule.

3.8. Molecular docking.

The 3D interacting site of ligands within the binding site of both proteins is figured in Figure 10, and Hydrogen bond interactions for compound 4 with both proteins are shown in Figure 11. Cytochrome P450 3A4 has one hydrogen bond attractor formed between N and

TYR124 at a distance of 2.73 Å. The molecular docking Score of the title compounds is -6.64 kcal/mol (Table 5). Acetylcholinesterase has one hydrogen bond donor formed between O and THR309 TYR124 at a distance of 1.90 Å. The molecular docking Score of the title compounds is -5.69 kcal/mol. It clearly shows that the synthesized compounds inhibit both of the two proteins.

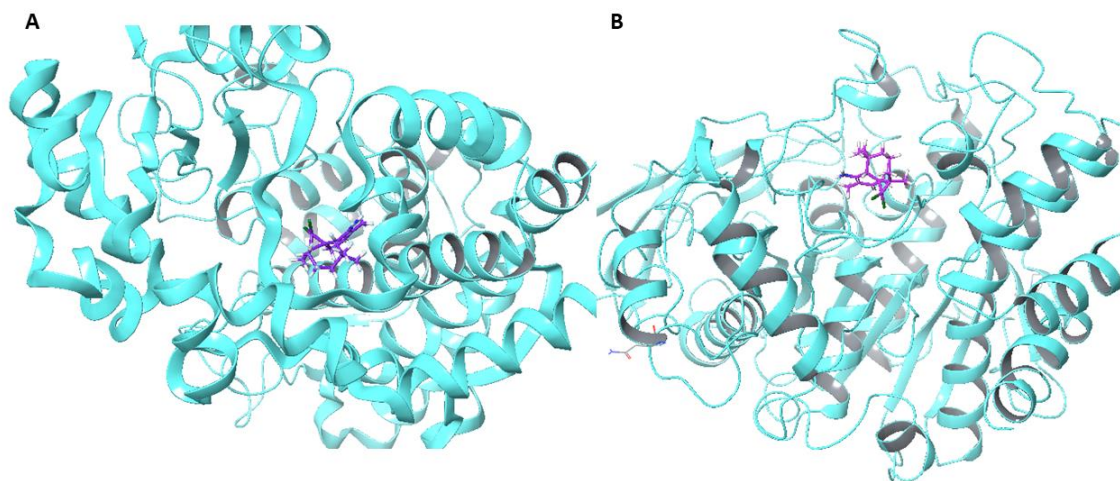


Figure 10. The compound 4 in the binding site of (A) Cytochrome P450 3A4 and (B) Acetylcholinesterase.

Table 5. The binding affinity of compound 4 with the Acetylcholinesterase and Cytochrome P450 3A4.

Protein	PDB CODE	Docking Score	MM/GBSA
Acetylcholinesterase	4ey7	-6,64	-7,301
Cytochrome P450 3A4	3nxu	-5,69	-7.30

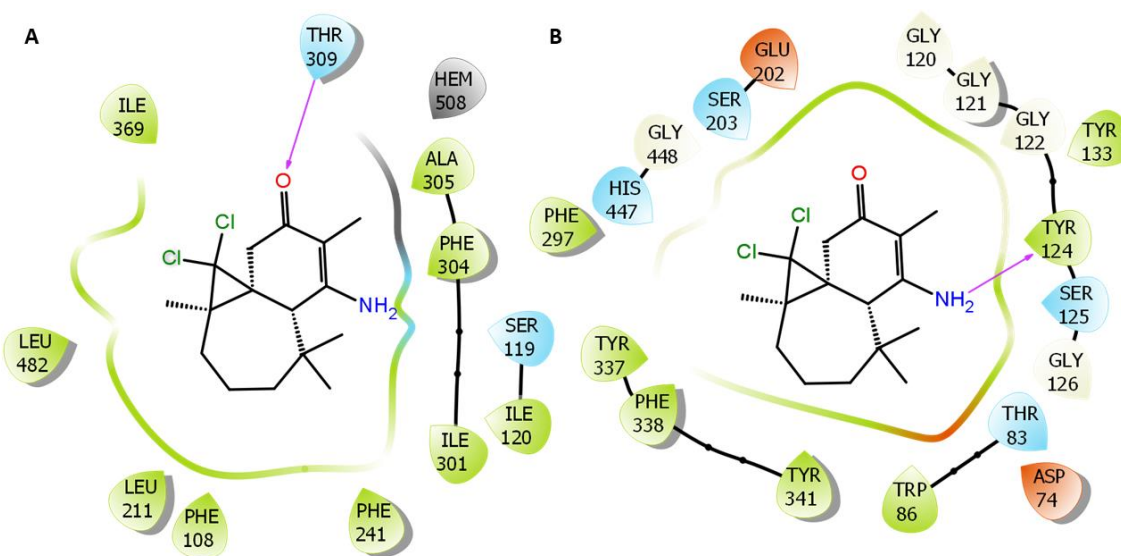


Figure 11. 3D structure of molecule 4 interacting with (A) Cytochrome P450 3A4, (B) Acetylcholinesterase.

4. Conclusions

A new himachalene derivative (1S,3R,8R)-11-amino-2,2-dichloro-3,7,7,10-tetramethyltricyclo[6.4.0.01,3]dodec-10-en-9-one (4) was synthesized and characterized by different techniques such as 1D NMR (¹H, ¹³C NMR, and DEPT), 2D NMR (HSQC, COSY, HMBC, and NOESY), FTIR spectra and X-ray structure determination. The single-crystal analysis shows that the product crystallizes in the monoclinic system with the P2/c space group. The optimized geometrical parameters (bond lengths, bond angles) within the DFT method were compared with experimental values, and a good agreement was achieved. NBO analysis

confirms that NH₂ participate as an electron-donating group, whereas C=O is an accepting group. The present study implies that the title compound can be used in the non-linear optical materials because β_{tot} of the title compound is around the 3 times greater than the urea. The binding affinities of this molecule to bind with Acetylcholinesterase and Cytochrome P450 3A4 were confirmed by Molecular docking, which showed the power linking of the molecule to these two proteins by scores calculation. These results are promising for studying a series of β -amino- α , β -unsaturated ketone (enantiomerically pure) syntheses from himachalenes.

Funding

We are grateful to Cadi Ayyad University, Chouaib Doukkali University, and Mohammed V University for providing financial support.

Acknowledgments

We are grateful to Cadi Ayyad University, Chouaib Doukkali University, and Mohammed V University for providing financial support. The authors are thankful to the Centro de Instrumentación Científica, Universidad de Granada, and Professor Ali Haidour Benamin for NMR experiments.

Conflicts of Interest

The authors declare that they have no conflict of interest.

References

1. Aberchane, M.; Fechtal, M.; Chaouch, A. Analysis of Moroccan Atlas Cedarwood Oil (*Cedrus atlantica* Manetti). *J Essent Oil Res* **2004**, *16*, 542-547, <https://doi.org/10.1080/10412905.2004.9698793>.
2. Chalchat, J.-C.; Garry, R.-P.; Miehet, A.; Benjilali, B. Essential Oil Components in Sawdust of *Cedrus atlantica* from Morocco. *J Essent Oil Res* **1994**, *6*, 323-325, <https://doi.org/10.1080/10412905.1994.9698386>.
3. Zoubi, Y.E.; Fouad, E.L.; Farah, A.; Taghzouti, K. Chemical composition and larvicidal activity of Moroccan Atlas Cedar (*Cedrus atlantica* Manetti) against *Culex pipiens* (Diptera: Culicidae). *J App Pharm Sci* **2017**, *7*, 030-034, <https://doi.org/10.7324/JAPS.2017.70704>.
4. Dakir, M.; Ait El Had. M.; Oukhrib, A.; Mazoir, N.; Benharref, A. Rearrangement of epoxide derivatives semisynthesized from β -himachalene using Lewis and bronsted acids catalysis. *Chemistry of Natural Compounds* **2020**, *56*, 663-669, <https://doi.org/10.1007/s10600-020-03116-w>.
5. Jaouadi, I.; Cherrad, S.; Bouyahya, A.; Koursaoui, L.; Satrani, B.; Ghanmi, M.; Chaouch, A. Chemical variability and antioxidant activity of *Cedrus atlantica* Manetti essential oils isolated from wood tar and sawdust. *Arabian Journal of Chemistry* **2021**, *14*, 103441, <https://doi.org/10.1016/j.arabjc.2021.103441>.
6. Daaboul, H.E.; Dagher, C.; Taleb, R.I.; Bodman-Smith, K.; Shebaby, W.N.; El-Sibai, M.; Daher, C.F., β -2-Himachalen-6-ol inhibits 4T1 cells-induced metastatic triple negative breast carcinoma in murine model. *Chemico-Biological Interactions* **2019**, *309*, 108703, <https://doi.org/10.1016/j.cbi.2019.06.016>.
7. Ait Lahcen, I.; Edder, Y.; Mallouk, S.; Boualy, B.; Karim, A. Synthesis and characterization of new secondary benzylamines derivatives of aryl-himachalene. *Chemical Papers* **2021**, *75*, 3207-3213, <https://doi.org/10.1007/s11696-021-01563-5>.
8. El Haib, A.; Benharref, A.; Parrès-Maynadié, S.; Manoury, E.; Urrutigoity, M.; Gouygou, M. Lewis acid- and Bronsted acid-catalyzed stereoselective rearrangement of epoxides derived from himachalenes: access to new chiral polycyclic structures. *Tetrahedron Asymmetry* **2011**, *22*, 101-108, <https://doi.org/10.1016/j.tetasy.2010.12.013>.
9. Aitouna, A.O.; Belghiti, M.E.; Eşme, A.; Aitouna, A.O.; Salah, M.; Chekroun, A.; El Alaoui El Abdallaoui, H.; Benharref, A.; Mazoir, N.; Zeroual, A.; Nejjari, C. Divulging the Regioselectivity of Epoxides in the Ring-Opening Reaction, and Potential Himachalene Derivatives Predicted to Target the Antibacterial Activities and SARS-CoV-2 Spike Protein with Docking Study. *Journal of Molecular Structure* **2021**, *1244*, 130864, <https://doi.org/10.1016/j.molstruc.2021.130864>.

10. Mori, K. Synthesis of (R)-ar-turmerone and its conversion to (R)-ar-himachalene, a pheromone component of the flea beetle: (R)-ar-himachalene is dextrorotatory in hexane, while levorotatory in chloroform. *Tetrahedron Asymmetry* **2005**, *16*, 685–692, <https://doi.org/10.1016/j.tetasy.2004.11.077>.
11. Bimoussa, A.; Oubella, A.; Laamari, Y.; Fawzi, M.; Hachim, M.E.; Ait Itto, M.Y.; Morjani, H.; Ketatni, El. M.; Mentre, O.; Auhmani, A. Hybrid of the 1,2,3-triazole nucleus and sesquiterpene skeleton as a potential antitumor agent: Hemisynthesis, Molecular structure, Hirshfeld surface analysis, DFT, in vitro cytotoxic and apoptotic effects. *Journal of Heterocyclic Chemistry* **2021**, *58*, 2334–2347, <https://doi.org/doi:10.1002/jhet.4359>.
12. Taleb, R.I.; Najm, P.; Shebaby, W.; Boulos, J.C.; Demirdjian, S.; Hariri, E.; Mroueh, M. β -2-himachalen-6-ol: A novel anticancer sesquiterpene unique to the Lebanese wild carrot. *J Ethnopharmacol* **2016**, *190*, 59–67, <https://doi.org/10.1016/j.jep.2016.05.053>.
13. Ez-Zriouli, R.; El Yacoubi, H.; Rochdi, A. Study of the sensitivity of certain bacteria–pathogenic human health-to atlas cedar essential oils and antibiotics. In *E3S Web of Conferences. EDP Sciences* **2021**, *319*, 01032, <https://doi.org/10.1051/e3sconf/202131901032>.
14. Daoubi, M.; Hernández-Galán, R.; Benharref, A.; Collado, I. G. Screening Study of Lead Compounds for Natural Product-Based Fungicides: Antifungal Activity and Biotransformation of $6\alpha,7\alpha$ -Dihydroxy- β -himachalene by *Botrytis cinerea*. *J Agric Food Chem* **2005**, *53*, 6673–6677, <https://doi.org/10.1021/jf050697d>.
15. Liu, Z.B.; Zhang, T.; Ye, X.; Liu, Z.Q.; Sun, X.; Zhang, L.L.; Wu, C.J. Natural substances derived from herbs or plants are promising sources of anticancer agents against colorectal cancer via triggering apoptosis. *Journal of Pharmacy and Pharmacology* **2021**, *rgab130*, <https://doi.org/10.1093/jpp/rgab130>.
16. Daaboul, H.E.; Daher, C.F.; Bodman-Smith, K.; Taleb, R.I.; Shebaby, W.N.; Boulos, J.; El-Sibai, M. Anti-tumor activity of β -2-himachalen-6-ol in colon cancer is mediated through its inhibition of the PI3K and MAPK pathways. *Chem Biol Interact.* **2017**, *275*, 162–170, <https://doi.org/10.1016/j.cbi.2017.08.003>.
17. Mahnashi, M.H.; Alyami, B.A.; Alqahtani, Y.S. Neuroprotective potentials of selected natural edible oils using enzyme inhibitory, kinetic and simulation approaches. *BMC Complement Med Ther* **2021**, *248*, <https://doi.org/10.1186/s12906-021-03420-0>.
18. Elias, A.; Shebaby, W.N.; Nehme, B.; Faour, W.; Bassil, B.S.; El Hakim, J.; Taleb, R.I. In Vitro and In Vivo Evaluation of the Anticancer and Anti-inflammatory Activities of 2-Himachalen-7-ol isolated from *Cedrus Libani*. *Sci Rep* **2019**, *9*, 1–9, <https://doi.org/10.1038/s41598-019-49374-9>.
19. Pinney, K. G.; Mejia, M. P.; Villalobos, V. M.; Rosenquist, B. E.; Pettit, G. R.; Verdier-Pinard, P.; Hamel, E. Synthesis and biological evaluation of aryl azide derivatives of combretastatin a-4 as molecular probes for tubulin. *Bioorg Med Chem* **2000**, *8*, 2417–2425, [https://doi.org/10.1016/S0968-0896\(00\)00176-0](https://doi.org/10.1016/S0968-0896(00)00176-0).
20. El-Kardocy, A.; Mustafa, M.; Ahmed, E. R.; Mohamady, S.; Mostafa, Y. A. Aryl azide-sulfonamide hybrids induce cellular apoptosis: synthesis and preliminary screening of their cytotoxicity in human HCT116 and A549 cancer cell lines. *Med Chem Res* **2019**, *28*, 2088–2098, <https://doi.org/10.1007/s00044-019-02438-x>.
21. Zaķis, J.M.; Ozols, K.; Novosjolova, I.; Vilšķersts, R.; Mishnev, A.; Turks, M. Sulfonyl Group Dance: A Tool for the Synthesis of 6-Azido-2-sulfonyl-purine Derivatives. *J Org Chem* **2020**, *85*, <https://doi.org/10.1021/acs.joc.9b03518>.
22. Gil, E.S.; da Silva, C.B.; Nogara, P.A.; da Silveira, C.H.; da Rocha, J.B.; Iglesias, B.A.; Rodembusch, F.S. Synthesis, photophysical characterization, CASSCF/CASPT2 calculations and CT-DNA interaction study of amino and azido benzazole analogues. *J Mol Liq* **2020**, *297*, 111938, <https://doi.org/10.1016/j.molliq.2019.111938>.
23. Yegorova, T.V.; Kysil, A.I.; Dyakonenko, V.V.; Levkov, I.V.; Karbovska, R.V.; Shishkina, S.V.; Voitenko, Z.V. Azido-tetrazole isomerism in 2,2-dimethyl-1-(1-methyl-1H-tetrazolo[5,1-a]isoindol-5-yl)propan-1-one. *J Mol Struct* **2020**, *1203*, 127469, <https://doi.org/10.1016/j.molstruc.2019.127469>.
24. Lazarova, N.; Zoghbi, S.S.; Hong, J.; Seneca, N.; Tuan, E.; Gladding, R.L.; Pike, V.W. Synthesis and evaluation of [N-methyl-11C]N-desmethyl-loperamide as a new and improved PET radiotracer for imaging P-gp function. *J Med Chem* **2008**, *51*, 6034–6043, <https://doi.org/10.1021/jm800510m>.
25. McIver, Z.A.; Kryman, M.W.; Choi, Y.; Coe, B.N.; Schamerhorn, G.A.; Linder, M.K.; Detty, M.R. Selective photodepletion of malignant T cells in extracorporeal photopheresis with selenorhodamine photosensitizers. *Bioorg Med Chem* **2016**, *24*, 3918–3931, <https://doi.org/10.1016/j.bmc.2016.05.071>.
26. Van de Walle, T.; Boone, M.; Van Puyvelde, J.; Combrinck, J.; Smith, P.J.; Chibale, K.; D'hooghe, M. Synthesis and biological evaluation of novel quinoline-piperidine scaffolds as antiplasmodium agents. *Eur J Med Chem.* **2020**, *198*, 112330, <https://doi.org/10.1016/j.ejmech.2020.112330>.
27. Wu, R.; Wang, L.; Kuo, H.C.D.; Shannar, A.; Peter, R.; Chou, P.J.; Kong, A. An Update on Current Therapeutic Drugs Treating COVID-19. *Curr Pharmacol Rep* **2020**, *1–15*, <https://doi.org/10.1007/s40495-020-00216-7>.
28. Pfister, J.R.; Makra, F.; Muehldorf, A.V.; Wu, H.; Nelson, J.T.; Cheung, P.; Slate, D.L. Methanodibenzosuberylpiperazines as potent multidrug resistance reversal agents. *Bioorg Med Chem Lett* **1995**, *5*, 2473–2476, [https://doi.org/10.1016/0960-894X\(95\)00426-T](https://doi.org/10.1016/0960-894X(95)00426-T).

29. Ekins, S.; Kim, R.B.; Leake, B.F.; *et al.* Application of three-dimensional quantitative structure-activity relationships of P-glycoprotein inhibitors and substrates. *Mol Pharmacol* **2002**, *61*, 974–981, <https://doi.org/10.1124/mol.61.5.974>.
30. Farooq, S.; Ngaini, Z. Chalcone derived benzoheterodiazepines for medicinal applications: A Two-pot and one-pot synthetic approach. *Journal of Heterocyclic Chemistry* **2021**, *58*, 1914–1928, <https://doi.org/10.1002/jhet.4337>.
31. Oukhrib, A.; Zaki, M.; Ait El Had, M.; El Karroumi, J.; Bouamama, H.; Benharref, A.; Urrutigoity, M. Synthesis of cyclopropane ring derivatives from natural β -himachalene and evaluation of their antimicrobial activity by bioautography. *RHAZES Green Appl Chem* **2019**, *6*, 61–70, <https://doi.org/10.48419/IMIST.PRSM/rhazes-v6.17798>.
32. Vogel, M.; Schmitz, R.P.H.; Hagel, S. Infectious disease consultation for Staphylococcus aureus bacteremia - A systematic review and meta-analysis. *J Infect* **2016**, *72*, 19–28, <https://doi.org/10.1016/j.jinf.2015.09.037>.
33. Amaye, I.J.; Harper, T.; Jackson-Ayotunde, P.L. Design and development of trifluoromethylated enaminone derivatives as potential anticonvulsants. *Journal of Fluorine Chemistry* **2021**, *251*, 109886, <https://doi.org/10.1016/j.jfluchem.2021.109886>.
34. Edafiogho, I.O.; Phillips, O.A.; Udo, E.E.; Samuel, S.; Rethish, B. Synthesis, antibacterial and anticonvulsant evaluations of some cyclic enaminones. *Eur J Med Chem*, **2009**, *44*, 967–975, <https://doi.org/10.1016/j.ejmech.2008.07.005>.
35. Edafiogho, I.O.; Qaddoumi, M.G.; Ananthakshmi, K. V. V.; Phillips, O. A.; Kombian, S. B. Synthesis, neuronal activity and mechanisms of action of halogenated enaminones. *Eur J Med Chem*. **2014**, *76*, 20–30, <https://doi.org/10.1016/j.ejmech.2014.02.002>.
36. Bimoussa, A.; Oubella, A.; Hachim, M.E.; Fawzi, M.; Itto, M.Y.A.; Mentre, O.; Auhmani, A. New enaminone sesquiterpenic: TiCl₄-catalyzed synthesis, spectral characterization, crystal structure, Hirshfeld surface analysis, DFT studies and cytotoxic activity. *Journal of Molecular Structure*, **2021**, *1241*, 130622, <https://doi.org/10.1016/j.molstruc.2021.130622>.
37. Dakir, M.; Auhmani, A.; Itto, M.Y.A.; Mazoir, N.; Akssira, M.; Pierrot, M.; Benharref, A. Optimization of Allylic Oxidation of (1S,3R,8R)-2,2-Dichloro-3,7,7,10-tetramethyltricyclo[6,4,0,0,1,3]dodec-9-ene. *Synth Commun* **2004**, *34*, 2001–2008, <https://doi.org/10.1081/SCC-120037912>.
38. Benharref, A.; El Ammari, L. Berraho, M. (1S,2R,8R)-2,2-Dichloro-3,7,7,10-tetra-methyltricyclo-[6.4.0.0,1,3]dodec-10-en-9-one. *Acta Cryst. E*. **2010**, *66*, o2911–o2911, <https://doi.org/10.1107/S1600536810040213>.
39. El Haib, A.; Benharref, A.; Parrès-Maynadié, S.; Maynadié, S.; Manoury, E.; Urrutigoity, M.; Gouygou, M.; Maynadié, S.; Manoury, E.; Urrutigoity, M.; Gouygou, M. Lewis acid- and Bronsted acid-catalyzed stereoselective rearrangement of epoxides derived from himachalenes: access to new chiral polycyclic structures. *Tetrahedron: Asymmetry* **2011**, *22*, 101–108, <https://doi.org/10.1016/j.tetasy.2010.12.013>.
40. Loubidi, M.; Agustin, D.; Benharref, A.; Poli, R. Solvent-free epoxidation of himachalenes and their derivatives by TBHP using [MoO₂(SAP)]² as a catalyst. *C R Chim* **2014**, *17*, 549–556, <https://doi.org/10.1016/j.crci.2014.01.023>.
41. Ait El Had, M.; Oukhrib, A.; Zaki, M.; Urrutigoity, M.; Benharref, A.; Chauvin, R. Versatile synthesis of cadalene and iso-cadalene from himachalene mixtures: Evidence and application of unprecedented rearrangements. *Chin Chem Lett* **2020**, *31*, 1851–1854, <https://doi.org/10.1016/j.cclet.2020.03.008>.
42. Eljamili, H.; Auhmani, A.; Dakir, M.; Lassaba, E.; Benharref, A.; Pierrot, M.; Riche, C. Oxydation et addition des dihalocarbènes sur le β -himachalène. *Tetrahedron Lett* **2002**, *43*, 6645–6648, [https://doi.org/10.1016/S0040-4039\(02\)01407-7](https://doi.org/10.1016/S0040-4039(02)01407-7).
43. Ourhriss, N.; Benharref, A.; Oukhrib, A.; Daran, J.C.; Berraho, M. (1S,3R,8R)-2,2-Di-chloro-3,7,7,10-tetra-methyl-tri-cyclo-[6.4.0.0,1,3]dodec-9-en-11-one. *Acta Crystallogr Sect E Struct Rep Online* **2013**, *69* (6), o830–o830, <https://doi.org/10.1107/S1600536813011781>.
44. Ait El had, M.; Benharref, A.; El Ammari, L.; Saadi, M.; Oukhrib, A.; Berraho, M. (1S,2R,8R)-11-Amino-2,2-di-chloro-3,7,7,10-tetra-methyl-tri-cyclo-[6.4.0.0,1,3]dodec-10-en-9-one. *IUCr Data* **2017**, *2*, x170255, <https://doi.org/10.1107/S2414314617002553>.
45. Ait El Had, M.; Oukhrib, A.; Zaki, M.; Taourirte, M.; Benharref, A.; Urrutigoity, M. BF₃-OEt₂-Catalyzed Rearrangement of Epoxy-Himachalenes: Access to New Biosourced N-Acetamide-Based Himachalenes. *Syn lett* **2021**, *32*, 309–315, <https://doi.org/10.1055/s-0040-1706545>.
46. Krause, L.; Herbst-Irmer, R.; Sheldrick, G.M.; Stalke, D. Comparison of silver and molybdenum microfocus X-ray sources for single-crystal structure determination. *J Appl Cryst* **2015**, *48*, 3–10, <https://doi.org/10.1107/S1600576714022985>.
47. Sheldrick, G.M. SHELXT – Integrated space-group and crystal-structure determination. *Acta Cryst A* **2015**, *71*, 3–8, <https://doi.org/10.1107/S2053273314026370>.
48. Farrugia, L.J. WinGX and ORTEP for Windows: an update. *J Appl Cryst* **2012**, *45*, 849–854, <https://doi.org/10.1107/S0021889812029111>.
49. Sheldrick, G.M. Crystal structure refinement with SHELXL. *Acta Cryst C* **2015**, *71*, 3–8, <https://doi.org/10.1107/S2053229614024218>.

50. Spackman, M.A.; Jayatilaka, D. Hirshfeld surface analysis. *Cryst Eng Comm* **2009**, *11*, 19–32, <https://doi.org/10.1039/B818330A>.
51. Spackman, M.A.; McKinnon, J.J. Fingerprinting intermolecular interactions in molecular crystals. *Cryst Eng Comm* **2002**, *4*, 378–392, <https://doi.org/10.1039/B203191B>.
52. Mackenzie, C.F.; Spackman, P.R.; Jayatilaka, D.; Spackman, M.A. CrystalExplorer model energies and energy frameworks: extension to metal coordination compounds, organic salts, solvates and open-shell systems. *IUCrJ* **2017**, *4*, 575–587, <https://doi.org/10.1107/S205225251700848X>.
53. Frisch, M.J.; Pople, J.A.; Binkley, J.S. Self-consistent molecular orbital methods 25. Supplementary functions for Gaussian basis sets. *J chem phys* **1984**, *80*, 3265–3269, <https://doi.org/10.1063/1.447079>.
54. Hachim, M.E.; Sadik, K.; Byadi, S.; Aboulmouhajir, A. Electronic investigation and spectroscopic analysis using DFT with the long-range dispersion correction on the six lowest conformers of 2,2,3-trimethyl pentane. *J Mol Model* **2020**, *26*, 168, <https://doi.org/10.1007/s00894-020-04430-4>.
55. Venkatesh, G.; Govindaraju, M.; Vennila, P.; Kamal, C. Molecular structure, vibrational spectral assignments (FT-IR and FT-RAMAN), NMR, NBO, HOMO–LUMO and NLO properties of 2-nitroacetophenone based on DFT calculations. *J Theor Comput Chem* **2016**, *15*, 1650007, <https://doi.org/10.1142/S0219633616500073>.
56. Muhammad, S.; Shehzad, R.A.; Iqbal, J.; Al-Sehemi, A.G.; Saravanabhavan, M.; Khalid, M. Benchmark study of the linear and non-linear optical polarizabilities in proto-type NLO molecule of para-nitroaniline. *J Theor Comput Chem* **2019**, *18*, 1950030, <https://doi.org/10.1142/S0219633619500305>.
57. Natarajan, S.; Shanmugam, G.; Dhas, S.A.M.B. Growth and characterization of a new semi organic NLO material: L-tyrosine hydrochloride. *Crys Res Tech* **2008**, *43*, 561–564, <https://doi.org/10.1002/crat.200711048>.
58. Thanthiriwatte, K.S.; Nalin, de Silva, K.M. Non-linear optical properties of novel fluorenyl derivatives—ab initio quantum chemical calculations. *J Mol Struct. THEOCHEM* **2002**, *617*, 169–175, [https://doi.org/10.1016/S0166-1280\(02\)00419-0](https://doi.org/10.1016/S0166-1280(02)00419-0).
59. Sagdinc, S.G.; Esme, A. Theoretical and vibrational studies of 4,5-diphenyl-2-2 oxazole propionic acid (oxaprozin). *Spectrochim. Acta A Mol Biomol Spectrosc* **2010**, *75*, 1370–1376, <https://doi.org/10.1016/j.saa.2010.01.004>.
60. Muthu, S.; Ramachandran, G. Spectroscopic studies (FTIR, FT-Raman and UV–Visible), normal coordinate analysis, NBO analysis, first order hyper polarizability, HOMO and LUMO analysis of (1R)-N-(Prop-2-yn-1-yl)-2,3-dihydro-1H-inden-1-amine molecule by ab initio HF and density functional methods. *Spectrochim Acta A Mol Biomol Spectrosc* **2014**, *121*, 394–403, <https://doi.org/10.1016/j.saa.2013.10.093>.
61. Morris, G.M.; Huey, R.; Indstrom, W.; Sanner, M.F.; Belew, R.K.; Goodsell, D.S.; Olson, A. AutoDock4 and AutoDockTools4: Automated docking with selective receptor flexibility. *J Comput Chem* **2009**, *30*, 2785–2791, <https://doi.org/10.1002/jcc.21256>.
62. Byadi, S.; Hachim, M.E.; Sadik, K.; Podlipnik, Č.; Aboulmouhajir, A. Fingerprint-based 2D-QSAR Models for Predicting Bcl-2 Inhibitors Affinity. *Lett Drug Des Disco* **2020**, *17*, 1206, <https://doi.org/10.2174/1570180817999200414155403>.
63. Watts, K.S.; Dalal, P.; Murphy, R.B.; Sherman, W.; Friesner, R.A.; Shelley, J.C. ConfGen: A Conformational Search Method for Efficient Generation of Bioactive Conformers. *J Chem Inf Model* **2010**, *50*, 534–546, <https://doi.org/10.1021/ci100015j>.
64. Filimonov, D.A.; Lagunin, A.A.; Glorizova, T.A.; Rudik, A.V.; Druzhilovskii, D.S.; Pogodin, P.V.; Poroikov, V.V. Prediction of the Biological Activity Spectra of Organic Compounds Using the Pass Online Web Resource. *Chem Heterocycl Comp* **2014**, *50*, 444–457, <https://doi.org/10.1007/s10593-014-1496-1>.
65. Wu, A.W.; Revicki, D.A.; Jacobson, D.; Malitz, F.E. Evidence for reliability, validity and usefulness of the Medical Outcomes Study HIV Health Survey (MOS-HIV). *Qual Life Res* **1997**, *6*, 481–493, <https://doi.org/10.1023/a:1018451930750>.
66. Zeldin, D.C.; Foley, J.; Goldsworthy, S.M.; Cook, M.E.; Boyle, J. E.; Ma, J.; Wu, S. CYP2J subfamily cytochrome P450s in the gastrointestinal tract: expression, localization, and potential functional significance. *Mol Pharmacol* **1997**, *51*, 931–943, <https://doi.org/10.1124/mol.51.6.931>.
67. Bieche, I.; Narjoz, C.; Asselah, T.; Vacher, S.; Marcellin, P.; Lidereau, R.; de Waziers, I. Reverse transcriptase-PCR quantification of mRNA levels from cytochrome (CYP) 1, CYP2 and CYP3 families in 22 different human tissues. *Pharmacogenet genomics* **2007**, *17*, 731–742, <https://doi.org/10.1097/fpc.0b013e32810f2e58>.
68. Kahma, H.; Aurinsalo, L.; Neuvonen, M.; Katajamäki, J.; Paludetto, M.-N.; Viinamäki, J.; Launiainen, T.; Filppula, A.M.; Tornio, A.; Niemi, M.; Backman, J.T. An automated cocktail method for in vitro assessment of direct and time-dependent inhibition of nine major cytochrome P450 enzymes – application to establishing CYP2C8 inhibitor selectivity. *European Journal of Pharmaceutical Sciences* **2021**, *162*, 105810, <https://doi.org/10.1016/j.ejps.2021.105810>.
69. Matsumoto, S.; Yamazoe, Y. Involvement of multiple human cytochromes P450 in the liver microsomal metabolism of astemizole and a comparison with terfenadine. *Br J Clin Pharmacol* **2001**, *51*, 133–142, <https://doi.org/10.1111/j.1365-2125.2001.01292.x>.

70. Hashizume, M.; Shimada, M.; Tomikawa, M.; Ikeda, Y.; Takahashi, I.; Abe, R.; Sugimachi, K. Early experiences of endoscopic procedures in general surgery assisted by a computer-enhanced surgical system. *Surg Endosc* **2002**, *16*, 1187–1191, <https://doi.org/10.1007/s004640080154>.
71. Leow, J.W.H.; Verma, R.K.; Lim, A.B.H.; Fan, H.; Chan, E.C.Y. Atypical kinetics of cytochrome P450 2J2: Epoxidation of arachidonic acid and reversible inhibition by xenobiotic inhibitors. *European Journal of Pharmaceutical Sciences* **2021**, *164*, 105889, <https://doi.org/10.1016/j.ejps.2021.105889>.
72. Fanni, D.; Pinna, F.; Gerosa, C.; Paribello, P.; Carpiello, B.; Faa, G.; Manchia, M. Anatomical distribution and expression of CYP in humans: Neuropharmacological implications. *Drug Development Research* **2021**, *82*, 628–667, <https://doi.org/10.1002/ddr.21778>.
73. Lafite, P.; André, F.; Zeldin, D.C.; Dansette, P.M.; Mansuy, D. Unusual regioselectivity and active site topology of human cytochrome P450 2J2. *Biochem* **2007**, *46*, 10237–10247, <https://doi.org/10.1021/bi700876a>.
74. Lee, C.A.; Jones, J.P.; Katayama, J.; Kaspera, R.; Jiang, Y.; Freiwald, S.; Totah, R. A. Identifying a Selective Substrate and Inhibitor Pair for the Evaluation of CYP2J2 Activity. *Drug Metab Dispos*, **2012**, *40*, 943–951, <https://doi.org/10.1124/dmd.111.043505>.
75. Montgomery, S.; Worswick, S. Photosensitizing drug reactions. *Clinics in Dermatology* **2021**, <https://doi.org/10.1016/j.clindermatol.2021.08.014>.
76. Colturato-Kido, C.; Lopes, R.M.; Medeiros, H.C.D.; Costa, C.A.; Prado-Souza, L.F.L.; Ferraz, L.S.; Rodrigues, T. Inhibition of Autophagy Enhances the Antitumor Effect of Thioridazine in Acute Lymphoblastic Leukemia Cells. *Life* **2021**, *11*, 365, <https://doi.org/10.3390/life11040365>.
77. Tuccinardi, T. What is the current value of MM/PBSA and MM/GBSA methods in drug discovery?. *Expert Opinion on Drug Discovery* **2021**, *16*, 1233–1237, <https://doi.org/10.1080/17460441.2021.1942836>.
78. Genheden, S.; Ryde, U., The MM/PBSA and MM/GBSA methods to estimate ligand-binding affinities. *Expert Opin Drug Discov* **2015**, *10* (5), 449–461, <https://doi.org/10.1517/17460441.2015.1032936>.
79. Ho, T.L.; Chein, R.J. Total Synthesis of (+)- β -Himachalene. *Helvetica Chimica Acta* **2006**, *89*, 231–239, <https://doi.org/10.1002/hlca.200690025>.
80. Oukhrib, A.; Zaki, M.; Ait El Had, M.; El Karroumi, J.; Bouamama, H.; Benharref, A.; Urrutigoity, M. Synthesis of cyclopropane ring derivatives from natural β -himachalene and evaluation of their antimicrobial activity by bioautography. *RHAZES Green Appl Chem* **2019**, *6*, 61–70, <https://doi.org/10.48419/IMIST.PRSM/rhazes-v6.17798>.
81. Ait El Had, M.; Oukhrib, A.; Zaki, M.; Urrutigoity, M.; Benharref, A.; Chauvin, R. Versatile synthesis of cadalene and iso-cadalene from himachalene mixtures: Evidence and application of unprecedented rearrangements. *Chin Chem Lett* **2020**, *31*, 1851–1854, <https://doi.org/10.1016/j.cclet.2020.03.008>.
82. El jamili, H.; Auhmani, A.; Dakir, M.; Lassaba, E.; Benharref, A.; Pierrot, M.; Riche, C. Oxydation et addition des dihalocarbènes sur le β -himachalène. *Tetrahedron Lett* **2002**, *43*, 6645–6648, [https://doi.org/10.1016/S0040-4039\(02\)01407-7](https://doi.org/10.1016/S0040-4039(02)01407-7).
83. Ourhriss, N.; Benharref, A.; Oukhrib, A.; Daran, J. C.; Berraho, M. (1S,3R,8R)-2,2-Di-chloro-3,7,7,10-tetra-methyl-tri-cyclo-[6.4.0.01,3]dodec-9-en-11-one. *Acta Cryst E* **2013**, *69*, o830–o830, <https://doi.org/10.1107/S1600536813011781>.
84. ChethanPrathap, K.N.; Lokanath, N.K. Three novel coumarin-benzenesulfonylhydrazide hybrids: Synthesis, characterization, crystal structure, Hirshfeld surface, DFT and NBO studies. *J Mol Struct* **2018**, *1171*, 564–577, <https://doi.org/10.1016/j.molstruc.2018.06.022>.
85. Hachim, M.E.; Sadik, K.; Byadi, S.; Van Alsenoy, C.; Aboulmouhajir, A. Ab initio study on the six lowest energy conformers of iso-octane: conformational stability, barriers to internal rotation, natural bond orbital and first-order hyperpolarizability analyses, UV and NMR predictions, spectral temperature sensitivity, and scaled vibrational assignment. *J Mol Model* **2019**, *25*, 1–19, <https://doi.org/10.1007/s00894-019-4105-5>.
86. Venkatesan, P.; Cerón, M.; Pérez-Gutiérrez, E.; Thamocharan, S.; Robles, F.; Ceballos, P.; Percino, M. J. Insights from QM/MM-ONIOM, PIXEL, NBO and DFT calculations: The molecular conformational origins for optical properties on (Z)-2-phenyl-3-(4-(pyridin-2-yl)-phenyl) acrylonitrile polymorphs. *J Mol Struct* **2020**, *1210*, 128016, <https://doi.org/10.1016/j.molstruc.2020.128016>.
87. Khajehzadeh, M.; Rajabi, M.; Rahmianasl, S. Synthesis, spectroscopic (UV–vis, FT-IR and NMR), solubility in various solvents, X–ray, NBO, NLO and FMO analysis of (L1) and [(L1)PdCl₂] complex: A comprehensive experimental and computational study. *J Mol Struct* **2019**, *1175*, 139–151, <https://doi.org/10.1016/j.molstruc.2018.07.084>.
88. Khajehzadeh, M.; Rajabi, M.; Rahmianasl, S. Synthesis, spectroscopic (UV–vis, FT-IR and NMR), solubility in various solvents, X–ray, NBO, NLO and FMO analysis of (L1) and [(L1)PdCl₂] complex: A comprehensive experimental and computational study. *J Mol Struct* **2019**, *1175*, 139–151, <https://doi.org/10.1016/j.molstruc.2018.07.084>.
89. Velraj, G.; Soundharam, S.; Sridevi, C. Structure, vibrational, electronic, NBO and NMR analyses of 3-methyl-2,6-diphenylpiperidin-4-one (MDPO) by experimental and theoretical approach. *J Mol Struct* **2014**, *1060*, 156–165, <https://doi.org/10.1016/j.molstruc.2013.12.040>.

90. Raja, M.; Raj, Muhamed, R.; Muthu, S.; Suresh. M. Synthesis, spectroscopic (FT-IR, FT-Raman, NMR, UV–Visible), NLO, NBO, HOMO-LUMO, Fukui function and molecular docking study of (E)-1-(5-bromo-2-hydroxybenzylidene) semicarbazide. *J Mol Struct.* **2017**, *1141*, 284–298, <https://doi.org/10.1016/j.molstruc.2017.03.117>.
91. Foster, J.P.; Weinhold, F. Natural hybrid orbitals. *J Am Chem Soc* **1980**, *102*, 7211-7218, <https://doi.org/10.1021/ja00544a007>.
92. Sekino, H.; Bartlett, R.J. Hyperpolarizabilities of the hydrogen fluoride molecule: A discrepancy between theory and experiment. *J Chem Phys* **1986**, *84*, 2726–2733, <https://doi.org/10.1063/1.450348>.

Supplementary material

1. Experimental and theoretical geometric parameters for compound 4

Table S1. Some selected experimental and theoretical geometric parameters for compound 4 (Å, °).

Geometric Parameters	Experimental values	DFT values
Bond (Å)		
C11—C22	1.762 (3)	1.800
C12—C22	1.762 (3)	1.789
O3—C16	1.235 (4)	1.225
N4—C39	1.340 (4)	1.375
C11—C23	1.512 (5)	1.527
C11—C7	1.515 (5)	1.521
C11—C22	1.513 (4)	1.512
C11—C12	1.531 (5)	1.546
C12—C22	1.505 (5)	1.521
C12—C13	1.513 (4)	1.518
C12—C37	1.525 (4)	1.534
C37—C39	1.512 (4)	1.518
C37—C32	1.587 (4)	1.598
C32—C33	1.530 (5)	1.542
C32—C40	1.526 (5)	1.543
C32—C29	1.553 (5)	1.552
C17—C18	1.509 (5)	1.507
C17—C39	1.375 (4)	1.365
C16—C17	1.424 (5)	1.456
C29—C26	1.517 (6)	1.539
C26—C23	1.543 (6)	1.544
C13—C16	1.503 (5)	1.529
Bond angles (°)		
C23—C11—C7	113.2 (3)	112.44
C23—C11—C22	119.2 (3)	119.26
C23—C11—C12	116.1 (3)	116.46
C22—C12—C13	118.6 (3)	118.93
C22—C12—C37	117.5 (2)	117.80
C13—C12—C37	112.2 (3)	112.49
C22—C12—C11	59.8 (2)	59.07
C39—C37—C12	108.5 (2)	108.96
C29—C32—C37	110.9 (3)	111.29
C11—C22—C11	121.1 (2)	120.88
C12—C22—C11	108.02 (17)	108.12
C16—C13—C12	114.0 (3)	114.06
O3—C16—C17	122.3 (4)	122.84
O3—C16—C13	117.5 (3)	118.55
C17—C16—C13	120.1 (3)	118.60
N4—C39—C17	121.1 (3)	120.99
N4—C39—C37	115.4 (2)	114.88
C17—C39—C37	123.5 (3)	124.04
C39—C17—C16	119.7 (3)	120.34
C39—C17—C18	121.2 (3)	121.53
C16—C17—C18	119.1 (3)	118.12
Torsion (°)		
C23—C11—C12—C22	-109.9 (3)	-109.95
C22—C12—C37—C39	-90.6 (3)	-92.41
C11—C12—C37—C32	72.5 (3)	70.35
C12—C37—C39—N4	150.0 (3)	153.46
C32—C37—C39—N4	-82.0 (3)	-76.49
N4—C39—C17—C16	-179.7 (3)	-177.14
N4—C39—C17—C18	0.5 (5)	1.48
C37—C39—C17—C18	-177.4 (3)	-178.06

Geometric Parameters	Experimental values	DFT values
C29—C26—C23—C11	36.1 (5)	36.66
C13—C12—C22—C12	2.4 (4)	1.58
C13—C12—C22—C11	-137.0 (3)	-138.34
C23—C11—C22—C12	-145.7 (3)	-144.71
C23—C11—C22—C11	6.0 (5)	-5.76
C39—C17—C16—O3	-174.6 (3)	-173.49

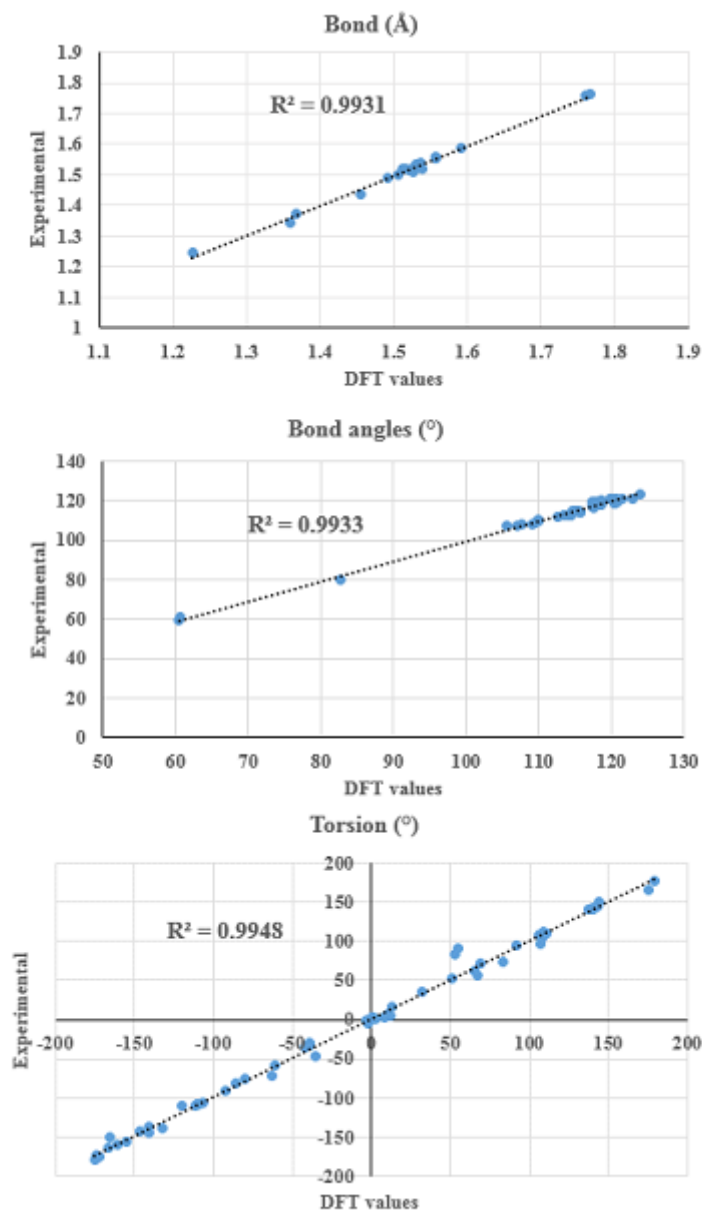


Figure S1. Correlation between experimental and theoretical geometric parameters for compound **4** (Å, °).

2. NLO calculations

Their electronic energy sensitivity to an external electric field F_i is expressed as follows:

$$E = E^{\circ} - \mu_i F_i - \frac{1}{2} \alpha_{ij} F_i F_j - \frac{1}{6} \beta_{ijk} F_i F_j F_k$$

where E^0 is the electronic energy of the unperturbed molecule, F_i is the external field at the origin, μ_i , α_{ij} and β_{ijk} are the components of dipole moment, polarizability and first order hyperpolarizability respectively. The total static dipole moment μ , the mean polarizability α_0 , the anisotropy of the polarizability α and the mean first order hyperpolarizability β_{tot} , using the x, y and z components are defined as:

Dipole moment

$$\mu = (\mu_x^2 + \mu_y^2 + \mu_z^2)^{1/2}$$

Static Polarizability

$$\alpha_0 = (\alpha_{xx} + \alpha_{yy} + \alpha_{zz})/3$$

Total Polarizability

$$\alpha = 2^{-1/2} [(\alpha_{xx} - \alpha_{yy})^2 + (\alpha_{yy} - \alpha_{zz})^2 + (\alpha_{zz} - \alpha_{xx})^2 + 6\alpha_{xy}^2 + 6\alpha_{xz}^2 + 6\alpha_{yz}^2]^{1/2}$$

First order Polarizability

$$\beta_{tot} = [(\beta_{xxx} + \beta_{xyy} + \beta_{xzz})^2 + (\beta_{yyx} + \beta_{yzz} + \beta_{yxx})^2 + (\beta_{zzx} + \beta_{zxx} + \beta_{zyy})^2]^{1/2}$$

The calculations of the total molecular dipole moment (μ), linear polarizability (α) and first-order hyperpolarizability (β) from the Gaussian output have been explained in detail previously.

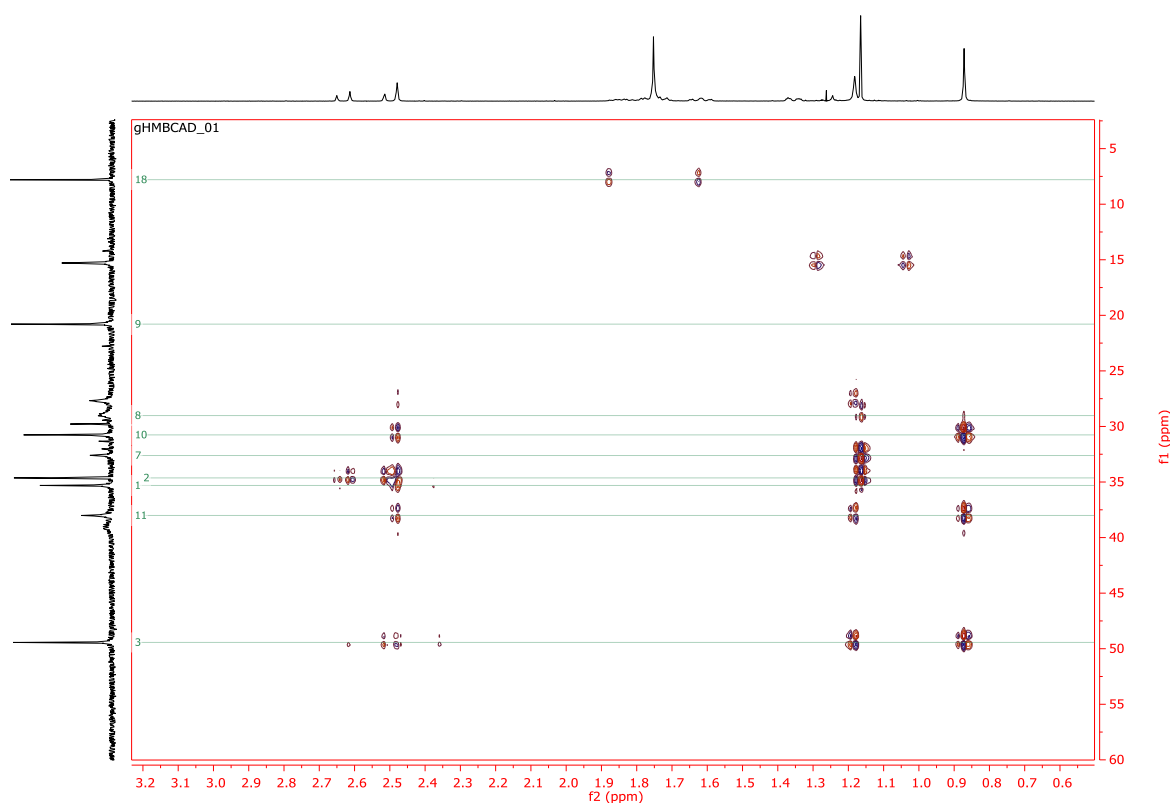


Figure S2. HMBC Spectrum of product **4**.

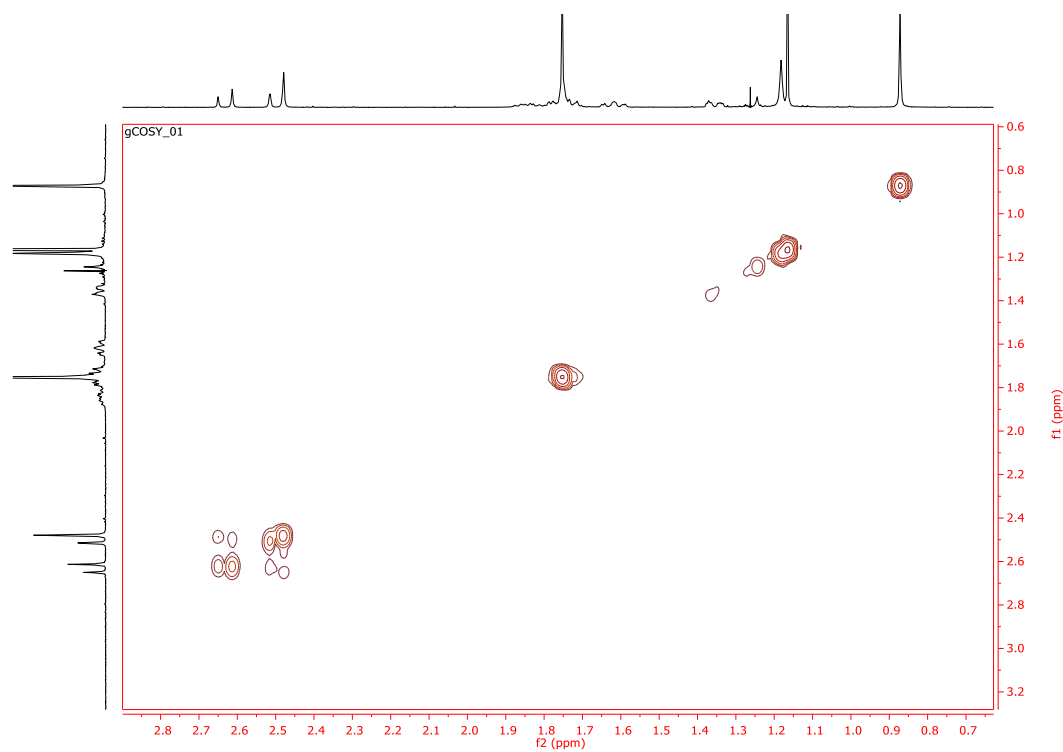


Figure S3. COSY Spectrum of product **4**.